



## RESEARCH ARTICLE

10.1029/2018PA003331

### Key Points:

- East Asian summer monsoon intensified in MIS 5, MIS 7, MIS 9, and MIS 11 when the Tsushima Current flowed into an unrestricted normal marine Japan Sea
- East Asian winter monsoon dominated MIS 2, MIS 4, MIS 6, and MIS 8 when sea level lows restricted the Japan Sea causing low-salinity and oxygen conditions
- Reduced oxygen stratified, low-salinity, and higher productivity oceanic conditions characterize Terminations TV, TIII, TII, and TI

### Supporting Information:

- Supporting Information S1
- Table S1
- Table S2

### Correspondence to:

S. J. Gallagher,  
sjgall@unimelb.edu.au

### Citation:

Gallagher, S. J., Sagawa, T., Henderson, A., Saavedra-Pellitero, M., De Vleeschouwer, D., Black, H., et al. (2018). East Asian monsoon history and paleoceanography of the Japan Sea over the last 460,000 years. *Paleoceanography and Paleoclimatology*, 33, 683–702. <https://doi.org/10.1029/2018PA003331>

Received 21 JAN 2018

Accepted 4 JUN 2018

Accepted article online 13 JUN 2018

Published online 4 JUL 2018

## East Asian Monsoon History and Paleoceanography of the Japan Sea Over the Last 460,000 Years

Stephen J. Gallagher<sup>1</sup> , Takuya Sagawa<sup>2</sup> , Andrew C. G. Henderson<sup>3</sup>,  
Mariem Saavedra-Pellitero<sup>4</sup> , David De Vleeschouwer<sup>5</sup> , Heather Black<sup>6</sup>, Takuya Itaki<sup>7</sup> ,  
Sam Toucanne<sup>8</sup>, Maria-Angela Bassetti<sup>9</sup>, Steve Clemens<sup>10</sup>, William Anderson<sup>6</sup>,  
Carlos Alvarez-Zarikian<sup>11</sup> , and Ryuji Tada<sup>12</sup>

<sup>1</sup>School of Earth Sciences, University of Melbourne, Melbourne, Victoria, Australia, <sup>2</sup>Institute of Science and Engineering, Kanazawa University, Kanazawa, Japan, <sup>3</sup>School of Geography, Politics and Sociology, Newcastle University, Newcastle upon Tyne, UK, <sup>4</sup>Department of Geosciences, Universität Bremen, Bremen, Germany, <sup>5</sup>MARUM - Center for Marine Environmental Research, Universität Bremen, Bremen, Germany, <sup>6</sup>Earth and Environment Department, and Marine Sciences, Florida International University, Miami, FL, USA, <sup>7</sup>Geological Survey of Japan, National Institute of Advanced Industrial Science and Technology, Tsukuba, Japan, <sup>8</sup>Centre Bretagne, Institut Français de Recherche pour l'Exploitation de la Mer, Issy-les-Moulineaux, France, <sup>9</sup>Laboratoire CEFREM, Université de Perpignan, Perpignan, France, <sup>10</sup>Earth, Environmental, and Planetary Sciences, Brown University, Providence, RI, USA, <sup>11</sup>International Ocean Discovery Program, Texas A&M University, College Station, TX, USA, <sup>12</sup>Department of Earth and Planetary Science, The University of Tokyo, Tokyo, Japan

**Abstract** The Japan Sea is directly influenced by the Asian monsoon, a system that transports moisture and heat across southeast Asia during the boreal summer, and is a major driver of the Earth's ocean-atmospheric circulation. Foraminiferal and facies analyses of a 460-kyr record from Integrated Ocean Drilling Program Expedition 346 Site U1427 in the Japan Sea reveal a record of nutrient flux and oxygenation that varied due to sea level and East Asian monsoon intensity. The East Asian summer monsoon (EASM) was most intense during marine isotope stage (MIS) 5e, MIS 7e, MIS 9e, and MIS 11c when the Tsushima Warm Current flowed into an unrestricted well-mixed normal salinity Japan Sea, whereas East Asian winter monsoon (EAWM) conditions dominated MIS 2, MIS 4, MIS 6, and MIS 8 when sea level minima restricted the Japan Sea resulting in low-salinity and oxygen conditions in the absence of Tsushima flow. Reduced oxygen stratified, low-salinity, and higher productivity oceanic conditions characterize Terminations TV, TIII, TII, and TI when East China Sea coastal waters breached the Tsushima Strait. Chinese loess, cave, and Lake Biwa (Japan) and U1427 proxy records suggest EASM intensification during low to high insolation transitions, whereas the strongest EAWM prevailed during lowest insolation periods or high to low insolation transitions. Ice sheet/CO<sub>2</sub> forcing leads to the strongest EAWM events in glacial and enhanced EASM in interglacials. Mismatches between proxy patterns suggest that latitudinal and land/sea thermal contrasts played a role in East Asian monsoon variability, suggesting that a complex interplay between ice sheet dynamics, insolation, and thermal gradients controls monsoonal intensity.

## 1. Introduction

The semi-enclosed Japan Sea on the northwest margin of the Pacific (Figure 1) is an ideal region to investigate the interaction between the ocean, climate, and sea level variability. The oceanography of the region is influenced by the Asian monsoon, a system that transports moisture and heat across Southeast Asia during the boreal summer, and is a major driver of planetary atmospheric circulation (Cheng et al., 2016). The Japan Sea is primarily connected to the open ocean via two shallow straits (130- to 140-m deep), and because of this, it has been strongly affected by the consequences of Pleistocene glacio-eustatic variability. Previous studies based on the analyses of microfossil, sedimentary, and oxygen isotope proxies show that highly variable oxygenation and salinity conditions over the last 160 kys were driven by ice volume, primarily varying with eccentricity influence, and this affected East Asian summer monsoon (EASM) variability (Tada et al., 1999, 2018; Usami et al., 2013; Watanabe et al., 2007). The current well-mixed open ocean circulation mode of the present Japan Sea is similar to marine isotope stage (MIS) 5e (Tada et al., 1999), yet during glacial maxima the Japan Sea was isolated. This change caused the surface salinity to decrease (as a result of an imbalance between precipitation and evaporation), and the resulting density stratification caused reduced oxygen bottom waters in MIS 2 and MIS 6 (Oba et al., 1991; Tada, 1994; Tada et al., 1999; Usami et al., 2013). Periodic intrusions of lower salinity, nutrient-rich waters into the Japan Sea from the East China Sea

©2018. The Authors.

This is an open access article under the terms of the Creative Commons Attribution-NonCommercial-NoDerivs License, which permits use and distribution in any medium, provided the original work is properly cited, the use is non-commercial and no modifications or adaptations are made.

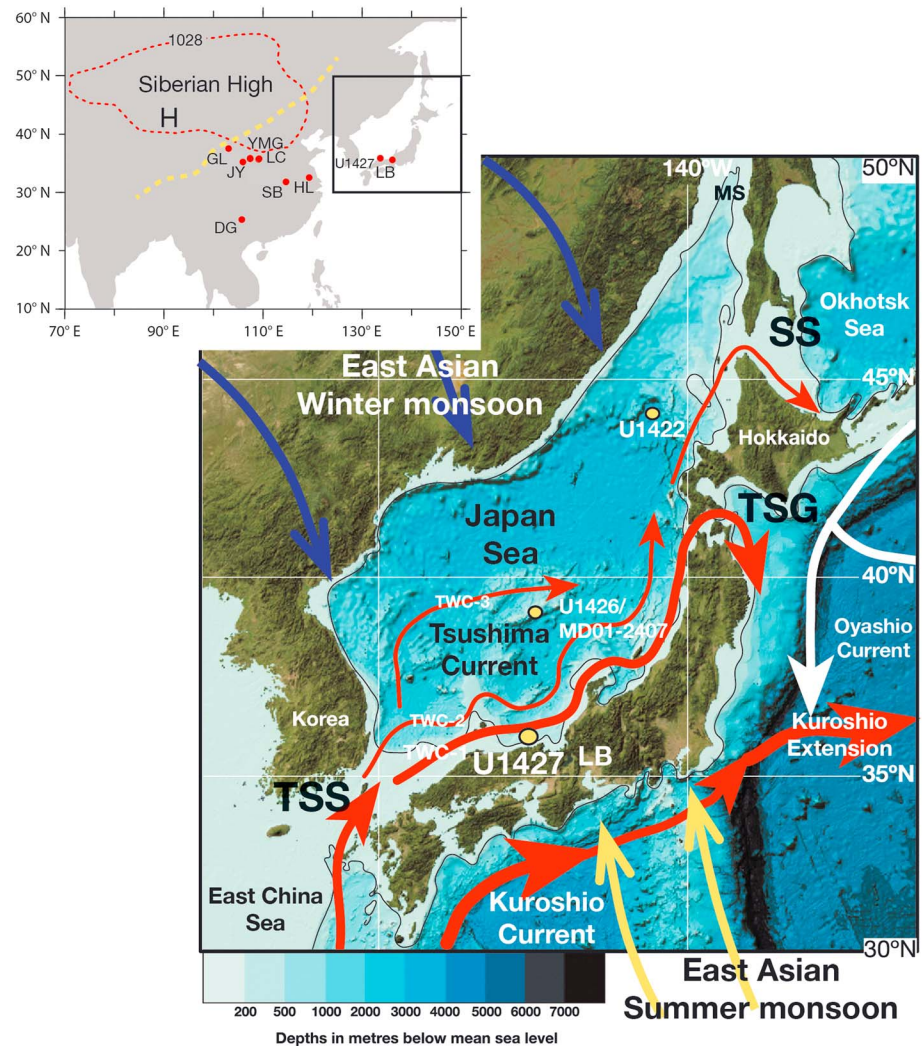


**Figure 1.** Location of IODP Expedition 346 Site U1427. The path of the Tsushima and Kuroshio Current and extension around Japan is shown. Tsushima Warm Current nomenclature (TWC-1 to TWC-3) is from Tada et al. (2015a). Base map adapted from General Bathymetric Chart of the Oceans ([www.gebco.net](http://www.gebco.net)). LB = Lake Biwa; MS = Mamiya Strait; TSS = Tsushima Strait; SS = Soya Strait; TSG = Tsuguru Strait. The inset map shows the center (H) of the Siberian High, and the dashed red line the area with 1,028 hPa of mean sea level pressure (adapted from Hao et al., 2012). The yellow dashed line is the northern limit of the summer monsoon front (Sun et al., 2015). YMG = Yimiguan; LC = Luochuan loess sections (Hao et al., 2012); GL = Gulang; JY = Jingyuan loess sections (Sun et al., 2015); DG = Dongge; SB = Sanbao; HL = Hulu cave sections (Cheng et al., 2016).

from MIS 3 to MIS 5d were the result of an enhanced EASM that led to higher surface productivity and weaker oceanic circulation (Tada et al., 1999; Usami et al., 2013; Watanabe et al., 2007).

The oceanographic and climatic history of the Japan Sea prior to 160 kyrs is poorly constrained. The glacial to interglacial mode described for the Japan Sea is interpreted to have likely started with the onset of the large-amplitude climate cycles during the Middle Pleistocene Transition at ~0.8 Ma (Tada, 1994). Tsushima Warm Current (TWC) inflow via an open Tsushima Strait has intermittently occurred over the last few million years during highstands (Gallagher et al., 2015; Hoiles et al., 2012; Itaki, 2016; Kitamura et al., 2001). Longer-term climate records adjacent to Site U1427 from Lake Biwa (LB; Figure 1), central Japan (Nakagawa et al., 2008), and Chinese loess (Hao et al., 2012; Sun et al., 2015; Figure 1) records show that 100-kyr eccentricity and 41-kyr obliquity cycles dominate monsoon intensity and precipitation.

The relationship between these terrestrial climate records and 460-kyr oceanographic history of the Japan Sea offers tantalizing glimpses into the complex interaction between sea level and monsoonal dynamics in the Japan Sea. Similarly, multiple proxies reveal a highly variable ventilation history over this period.

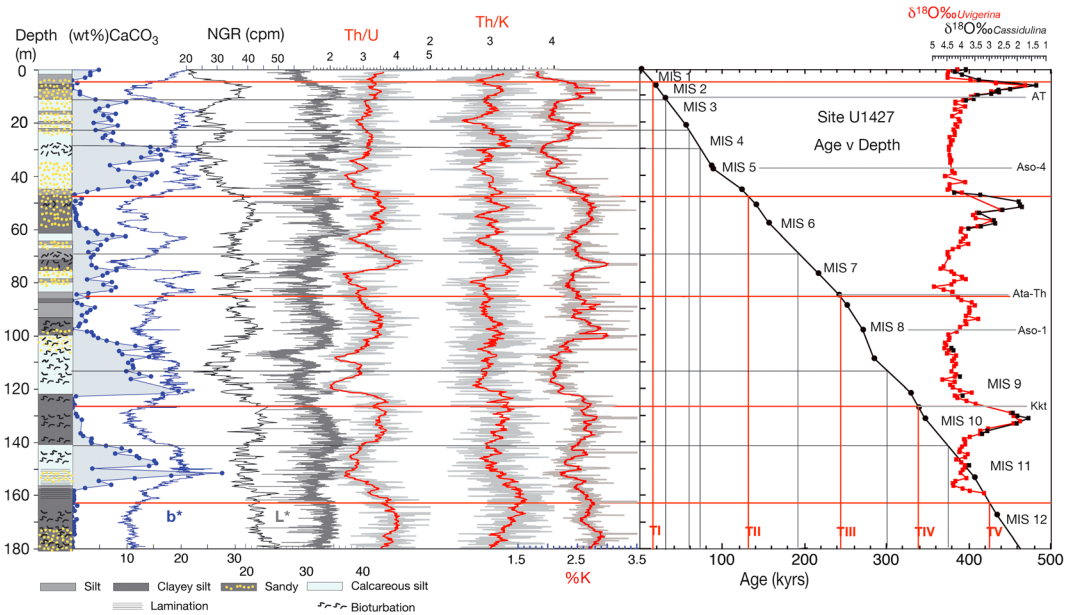


**Figure 2.** Lithostratigraphy of the upper 180 m of Site U1427 with downhole physical properties. The age-depth curve shows marine isotope stages, benthic foraminiferal isotope data, and tephrochronology (Table 1) from Sagawa et al. (2018). NGR cpm = natural gamma ray counts per minute.

Integrated Ocean Drilling Program (IODP) Expedition 346 cored a series of sites in 2013 in the Japan Sea to obtain a continuous 5 Ma-sedimentary record of Asian monsoon history (Tada et al., 2015a, 2018). The focus of this study is IODP Site U1427 (Tada et al., 2015b, 2018; Sagawa et al., 2018), adjacent to the western Japanese coastline underneath the main branch of the TWC (Figure 1). We use sedimentary physical properties and facies, and benthic and planktic foraminiferal assemblage analyses of this section to reveal a high-resolution paleoceanographic history of the southern Japan Sea over the last 460 kyrs. The data reveal the strong relationship between sea level, monsoon, and ocean variability over the last five glacial/interglacial cycles.

## 2. Oceanographic Setting

The Japan Sea is a semiclosed marginal sea in the northwest Pacific. Its area exceeds 1,000,000 km<sup>2</sup> with an average depth of 1350 m (Oba et al., 1991; Tada, 1994; Tada et al., 1999). The sea is connected to the East China Sea through the Tsushima Strait (< 140 m), to the Pacific Ocean via the Tsugaru Strait (< 130 m), and to the Okhotsk Sea through the Soya (< 55 m) and Mamiya (< 12 m) Straits (Figure 1). The modern surface water of the Japan Sea is strongly influenced by the TWC, an offshoot of the Kuroshio Current (Figure 1; Gallagher et al., 2009, 2015). The warm saline Kuroshio Current mixes with the less saline nutrient-rich East China Sea Coastal Water (ECSCW) south of Japan (Figure 1; Qiu, 2001; Usami et al., 2013) before flowing into the Japan Sea via the Tsushima Strait as the TWC (Figure 1). Today, the only oceanic water flowing into the Japan Sea is via the warm TWC, with surface velocities ranging from 0.3 to 0.4 m/s and volumes from 1.1 to 2.6 Sverdrups (10<sup>6</sup> m<sup>3</sup>/s) in the Tsushima Strait flowing northward along the Coast of Honshu Island (Takikawa & Yoon, 2005). The majority of the current flows out through the Tsugaru Strait to the Pacific Ocean. Some of the current flows out through the Soya Strait to the Okhotsk Sea, the rest flows to the northern Japan Sea where it sinks to the bottom as it cools down to temperatures near 0 °C (Gamo & Horibe, 1983; Moriyasu, 1972; Suda, 1932). This low temperature (0.1–0.3 °C), low salinity (34), and high dissolved oxygen concentration (>210 μmol/kg) homogenous water mass is the Japan Sea Proper Water (JSPW). JSPW dominates depths below 300 m (Oba et al., 1991; Ohta et al., 2015; Tada et al., 1999) and bathes the region around IODP Site U1427.

## 3. Site Location and Methods

IODP Expedition 346 Site U1427 was cored in the Yamato Basin at 35°57.92'N, 134°26.06'E (Figure 1) at 337-m water depth recovering nearly 550 m of continuous sediment core below sea floor. This work focuses on

**Table 1**  
The Age-Depth Model Used in Figure 2 From Sagawa et al. (2018)

U1427 depth (m)	Age (ka)	Source	Datums	Reference
0	0	Core top		
6.01	18	benthic $\delta^{18}\text{O}$	MIS 2	Lisiecki and Raymo (2005)
10.69	30.0	tephra	AT	Smith et al. (2013)
20.98	54	bio-event	LO <i>Lychnocanoma sakaii</i>	Itaki et al. (2007)
36.09	85	bio-event	LO <i>Amphimelissa setosa</i>	Itaki et al. (2007)
37.54	87.0	tephra	Aso-4	Aoki (2008)
45.10	123	subtropical microfossil	MIS 5e	Lisiecki and Raymo (2005)
50.78	140	benthic $\delta^{18}\text{O}$	MIS 6a	Lisiecki and Raymo (2005)
57.84	155	benthic $\delta^{18}\text{O}$	MIS 6c	Lisiecki and Raymo (2005)
76.67	217	subtropical microfossil	MIS 7c	Lisiecki and Raymo (2005)
84.67	242	tephra (tied to U1429)	Ata-Th	
88.51	252	benthic $\delta^{18}\text{O}$	MIS 8a	Lisiecki and Raymo (2005)
97.68	270.2	tephra (tied to U1429)	Aso-1	
108.55	285	subtropical microfossil	MIS 9a	Lisiecki and Raymo (2005)
121.27	329	subtropical microfossil	MIS 9e	Lisiecki and Raymo (2005)
126.74	339.2	tephra (tied to U1429)	Kkt	
131.00	346	benthic $\delta^{18}\text{O}$	MIS 10a	Lisiecki and Raymo (2005)
153.05	406	subtropical microfossil	MIS 11c	Lisiecki and Raymo (2005)
167.2	433	b*	MIS 12a	Lisiecki and Raymo (2005)
191.57	491	subtropical microfossil	MIS 13a	Lisiecki and Raymo (2005)
198.94	525	subtropical microfossil	MIS 13c	Lisiecki and Raymo (2005)

Note. MIS = marine isotope stage.

detailed analyses of the top 180 m of this core (Figure 2). The lithology of the facies (Figure 2) was compiled from detailed shipboard core descriptions with interpretations of standard IODP shipboard physical property measurements (Tada et al., 2015a) and additional %carbonate data. Natural Gamma Radiation (NGR) logging was carried out on whole round core though the section. Postcruise U, Th, and K elemental concentrations were extracted from the shipboard NGR spectral measurements using a NGR-spectrum integration method (see De Vleeschouwer et al., 2017). A color reflectance spectrometer (Ocean Optics sensor) measured L\* lightness, a\* redness (positive) versus greenness (negative), and b\* yellowness (positive) versus blueness (negative) of the strata. Carbonate content analyses using the volumetric technique of Wallace et al. (2002) were carried out on 165 samples (Figure 2). b\* is illustrated (Figure 2) as it was found to be related to relative carbonate content (Tada et al., 2015b). The age model used in this work (Figure 2 and Table 1) is from Sagawa et al. (2018) who constructed a detailed calibration using radiolarian biostratigraphy, tephrochronology, and benthic foraminiferal isotope correlations to the LR2004 stack (Lisiecki & Raymo, 2005).

The sediment size is mainly silt (Figure 2), subdivided it into three main facies types: calcareous silt (with relatively high %carbonate ( $\geq 5\%$ ) and b\* and low NGR values), clayey silt (with high NGR values and low %carbonate [ $< 5\%$ ] and b\*), and silt (low NGR values and low %carbonate). When a sand component was recognized during visual core description, the facies were designated *sandy*. One hundred and sixty-three samples were processed for foraminifera by standard microfossil techniques for paleoenvironmental analyses (with emphasis on sea surface conditions and paleoproductivity proxies). The samples were split (using a microsplitter) into several fractions. Quantitative benthic and planktic assemblage data were compiled from the  $\geq 150 \mu\text{m}$  fraction. The foraminiferal data are expressed as a percentage of the total fauna (e.g., %plankton and %miliolids) or as a percentage of the calcareous benthic or planktic assemblage. Foraminiferal concentrations are expressed as numbers of foraminifera per gram of dry sediment (Figure 3).

Conditions within and on the seabed are interpreted using facies and benthic foraminiferal assemblage data. Sea surface conditions are determined using planktic foraminiferal assemblage data (Figures 4 and 5) and comparisons with modern regional analogs (Domitsu & Oda, 2005; Kuroyanagi & Kawahata, 2004). Benthic foraminifera (Figures 6 and 7) are sensitive indicators of bottom water conditions as they show variability related to dissolved oxygen and nutrient availability worldwide (Gooday, 2003; Jorissen, 1999; Jorissen

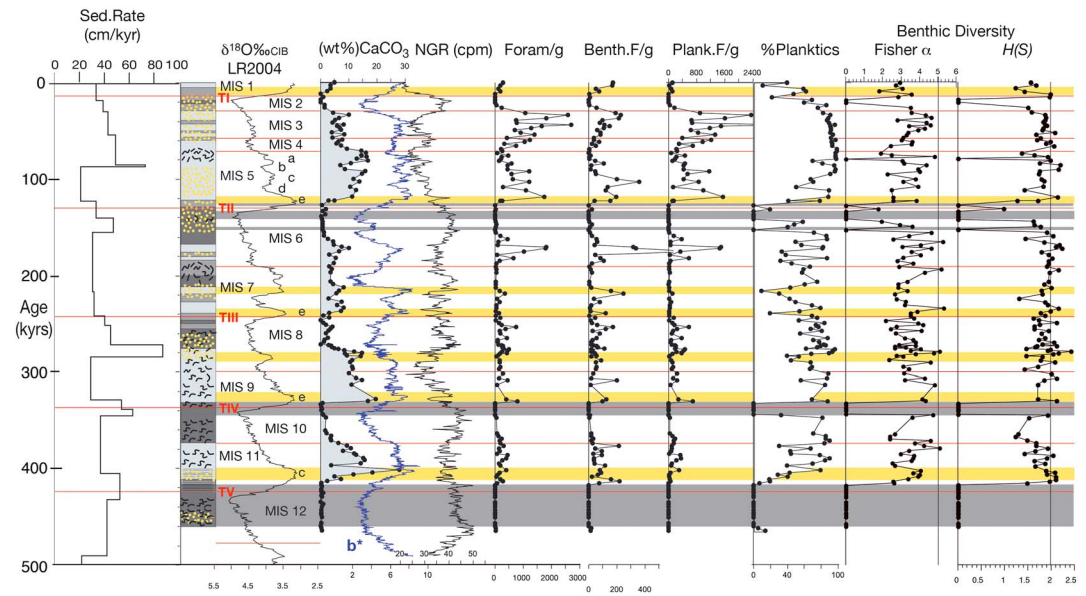


**Figure 3.** An age plot of the lithostratigraphy, foraminiferal concentration, and %planktics (expressed as percentage of the total foraminiferal fauna) in the upper 460 kyrs of Site U1427. Benth. F = benthic foraminifera and plank. F = planktic foraminifera. The yellow horizons are interglacial maxima in the LR2004 stack (Lisiecki & Raymo, 2005). The labeling uses the Railsback et al. (2015) nomenclature. The gray horizons are barren of foraminifera. The key to the log lithology and symbols is in Figure 2. The linear sedimentation rate (Sed.Rate) curve is from Sagawa et al. (2018). The benthic assemblage diversity uses the Fisher  $\alpha$  index and Shannon-Weaver indices,  $H(S) > 2$ , and Fisher  $\alpha > 5$  typify open marine shelf and deep sea environments.

et al., 2007; Kaiho, 1994). Specific benthic foraminifer assemblage comparisons (in this work, Table 2) to modern analogs off Japan (Fontanier et al., 2014) and in the Okhotsk Sea (Bubenschchikova et al., 2008, 2015) allow fossil assemblages to be interpreted in their regional context (cf. Usami et al., 2013), accounting for the relative isolation of the Japan Sea compared to more open ocean settings. The diversity indices used (Figure 3) are the Fisher  $\alpha$  index (Murray, 1991, 2006) and the Shannon-Weaver index  $H(S)$ ; Murray, 2006; Shannon & Weaver, 1949).  $H(S)$  takes into account the number of taxa in a sample and their equitability of distribution within that sample. The Shannon-Weaver index is calculated as follows:

$$H(S) = - \sum_{i=1}^S p_i \ln p_i$$

where  $H(S)$  = index of species diversity,  $S$  = the number of species, and  $p_i$  = proportion of total samples belonging to the  $i$ th species. Our data are compared to global faunal data, where  $H(S)$  values  $> 2$  and Fisher  $\alpha$  values  $> 5$  typify open marine shelfal and deep sea environments (Murray, 2006; the vertical lines in Figure 3), whereas values less than this are from more restricted marine and marginal marine environments. Bioturbation intensity is also strongly related to sea bed oxygenation (Watanabe et al., 2007). In this work the terms anoxic =  $0.1 \text{ O}_2 \text{ ml/L}$ , dysoxic =  $0.1\text{--}0.3 \text{ O}_2 \text{ ml/L}$ , suboxic =  $0.3\text{--}1.5 \text{ O}_2 \text{ ml/L}$ , and oxic =  $> 1.5 \text{ O}_2 \text{ ml/L}$  (sensu Kaiho, 1994).

## 4. Results

### 4.1. Facies and Physical Properties

The sediment facies at IODP Site U1427 are strongly cyclic (Figure 2).

From the base to the top we observe the following.

1. The lowest strata (below 156 m, MIS 11/MIS 12) are sandy clayey silt overlain by clayey silt and a unit of laminated silt. Color reflectance  $b^*$  increases up section while brightness ( $L^*$ ) and NGR values decrease associated with relatively high %K, Th/U, and Th/K ratios.

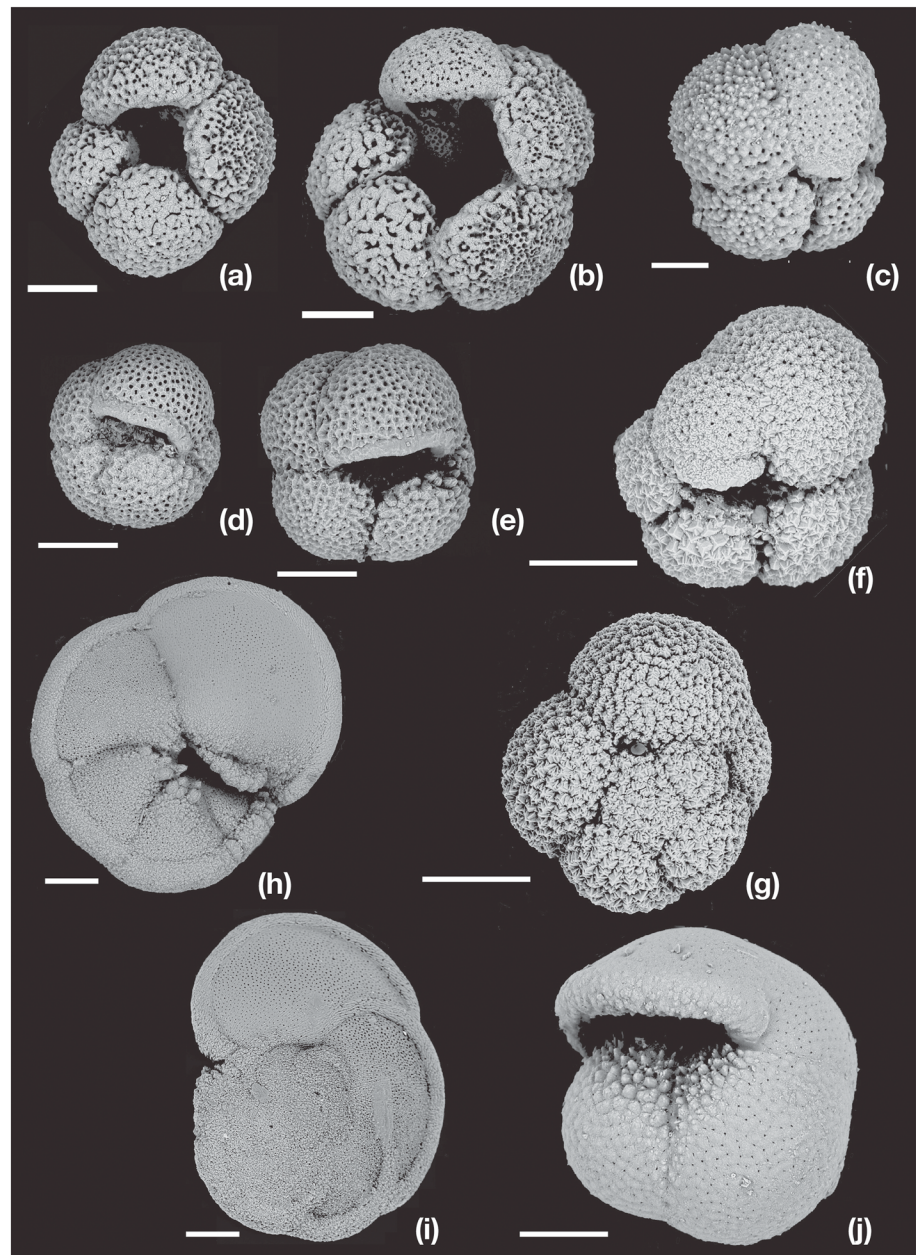


**Figure 4.** Planktic foraminifera in Pleistocene strata of Integrated Ocean Drilling Program Site U1427. The scale bar is 100  $\mu\text{m}$ . (a) *Globigerina bulloides* (d'Orbigny, 1826: thick-walled form sensu Domitsu & Oda, 2005), log level 167.02 m. (b) *Globigerina umbilicata* Orr and Zaitzeff, 1971, 167.02 m. (c) *Globigerina quinqueloba* Natland, 1938, log level 61.27 m. (d and e) *Neogloboquadrina pachyderma* (Ehrenberg, 1861), log level 11.92 m. (f and g) *Neogloboquadrina incompta* (Cifelli, 1961), log level 0.04 m. (h and i) *Globorotalia tumida* (Brady, 1877), log level 145.57 m. (j) *Pulleniatina obliquiloculata* (Parker and Jones, 1862), log level 44 m.

2. From ~156 to 84 m (MIS 11 to MIS 8) the two cycles are composed of calcareous silt (with high  $b^*$ , low brightness  $L^*$ ) at the base, grading upward to a calcareous clayey silt and a silt unit. Brightness ( $L^*$ ); NGR values; and %K, Th/U, and Th/K ratios increase, and  $b^*$  values decrease into the mud-rich facies and reverse in the silt. Sections with sandy facies are present from ~158 to 150 m and ~108 to 98 m. Bioturbation intensity is generally high, although there is a laminated interval at the start of MIS 11 and occasional homogenous clayey silt and silt units near the end of MIS 10 and MIS 8.
3. The sedimentary facies in the interval above ~84 m (MIS 7 to MIS 6) show meter-scale variability: calcareous silt (with high  $b^*$  and low NGR values with low %K, Th/U, and Th/K ratios), alternate clayey silt

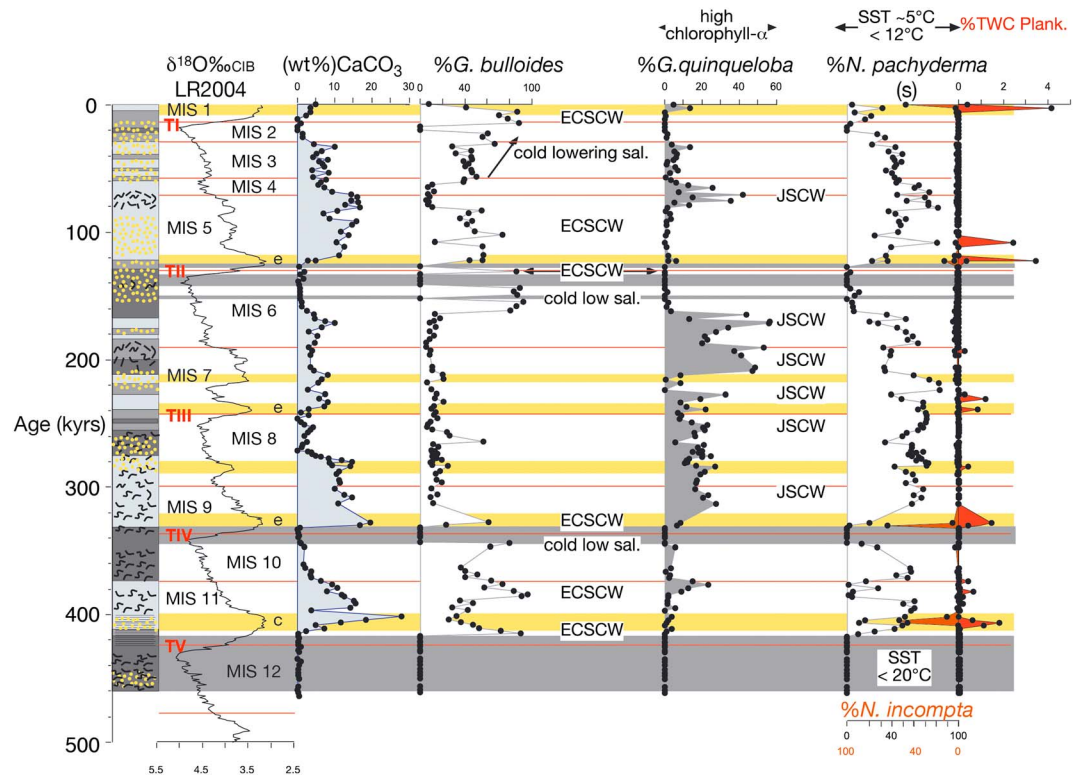


**Figure 5.** An age plot of the key planktic species in the upper 460 kyrs of Site U1427. *G.* = *Globigerina*, *N.* = *Neogloboquadrina*, and (s) = sinistral. ECSCW = East China Sea coastal waters; JSCW = Japan Sea coastal waters; SST = sea surface temperatures; and TWC plank. = Tsushima Warm Current planktic species. %values are expressed as a percentage of the total planktic fauna. MIS = marine isotope stage.

(with low  $b^*$ ; high  $L^*$  and NGR values; and high %K, Th/U, and Th/K ratios), and silt units. Sandy facies are present in MIS 7 and common in MIS 6. Intensely bioturbated horizons are present at ~70 m and 50 m. The upper cycle above ~50 m is a sandy calcareous silt that grades to a calcareous muddy silt (MIS 5 to MIS 4) overlain by a 15-m interval (MIS 3) of meter-scale silt/calcareous silt alternations. The uppermost 10 m (MIS 2 to MIS 1) is sandy silt that grades up section to clayey silt that is overlain by calcareous silt. NGR,  $L^*$ , and  $b^*$  values in the upper 50 m show similar patterns to facies variations to the underlying cycles. The facies in the upper cycle is relatively homogenous with one interval of intense bioturbation at ~30 m.

#### 4.2. Sedimentation Rates

Linear sedimentation rates increase from MIS 12 to Termination V and from MIS 10 to Terminations IV (Figure 3). Thereafter, values range from 20 to 40 cm/kyr with occasional maxima near the start of MIS 8 and just prior to Termination II. Values decrease from MIS 5 to present.

#### 4.3. Foraminiferal Assemblages

Foraminiferal abundance is low in U1427 with an average 300 foraminifera/g of sediment with a maximum of ~2,700 during MIS 3 (Figure 3). Abundance varies, intervals where foraminifera are absent or rare include MIS 12/base MIS 11, end of MIS 10/base MIS 9, end of MIS 7/base MIS 6, and end of MIS 6/base MIS 5 and MIS 2 (Figure 3). Foraminiferal concentration maxima >1,000 foraminifera/g of sediment are present in MIS 6, MIS 5e, MIS 5d, and from MIS 4 to MIS 3. In other intervals, foraminiferal abundance varies from 50 to 500 foraminifera/g. Maximum numbers of benthic foraminifera generally correspond to the abundance maxima described above; however, they are relatively common in MIS 11, near the start of MIS 9 and MIS 7. The relative abundance of planktic foraminifera varies markedly, ranging from 10% to 100% with an average of ~55% (Figure 3). With a mean value of 250 planktics/g of sediment, planktic foraminifera dominate the total foraminiferal concentration described above. Where foraminifera are present prior to MIS 5 the pattern of low

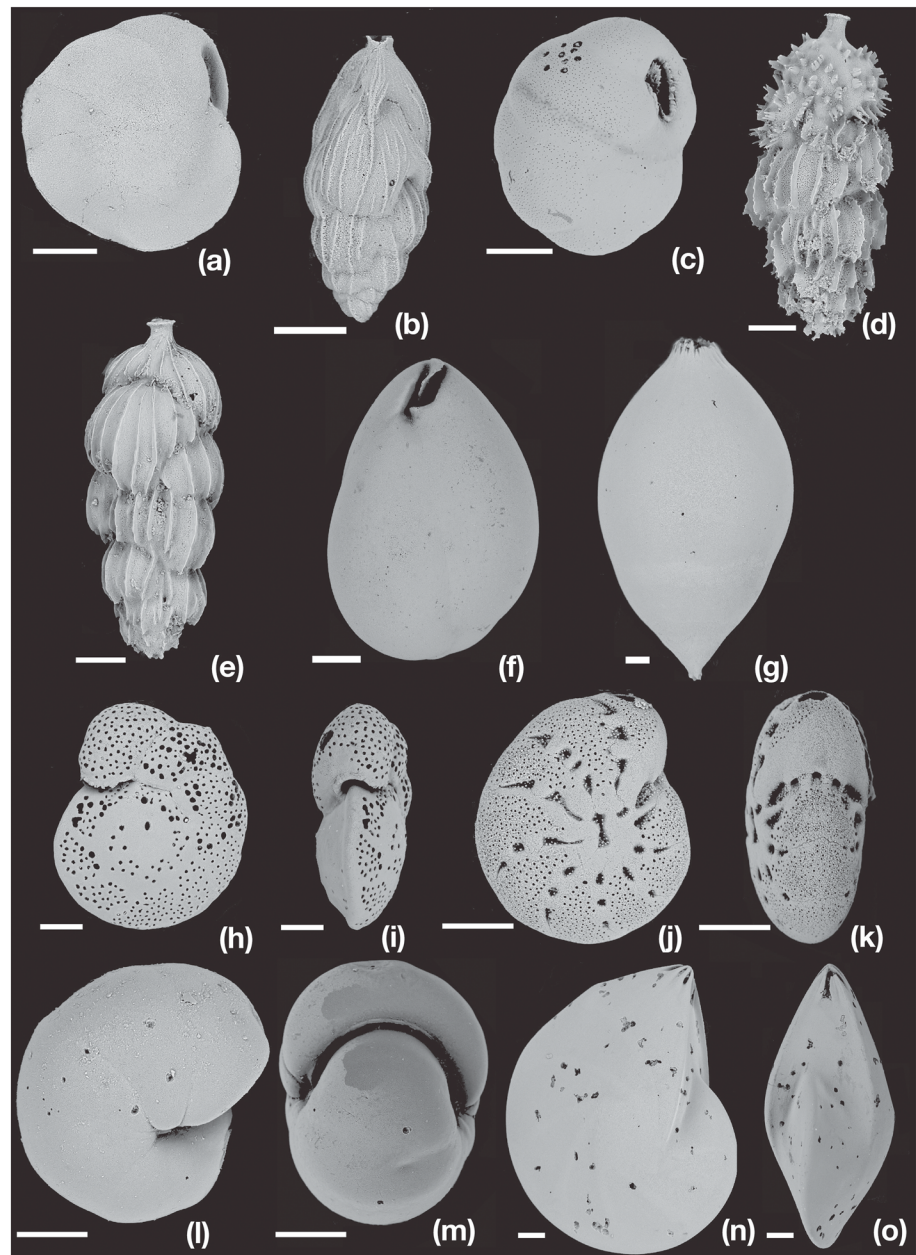


**Figure 6.** Benthic foraminifera in Pleistocene strata of Integrated Ocean Drilling Program Site U1427. The scale bar is 100  $\mu\text{m}$ . (a) *Islandiella norcrossi* (Cushman, 1933), log level 8.86 m. (b) *Trifarina angulosa* (Williamson, 1858), 167.02 m. (c) *Globocassidulina subglobosa* (Brady, 1861), log level 10.92 m. (d) Spinose-striate *Uvigerina* cf. *graciliformis* (sensu Fontanier et al., 2014), log level 61.27 m. (e) *Uvigerina akitaensis* Asano, 1950, log level 44 m. (f) *Globobulimina pacifica* Cushman, 1927, log level 167.02 m. (g) *Glandulina laevigata* (d'Orbigny, 1826), log level 167.02 m. (h and i) *Cibicides lobatulus* (Walker and Jacob, 1878), log level 2.98 m. (j and k) *Elphidium excavatum* (Terquem, 1875), log level 2.98 m. (l and m) *Pullenia bulloides* (d'Orbigny, 1846), log level 11.92 m. (n and o) *Lenticulina inornata*, log level 10.92 m.

and high planktic values follow  $b^*$  values with common benthic foraminifera during periods with higher  $b^*$  and %carbonate. The trend is similar from MIS 5, MIS 2, and MIS 1; however, the  $b^*$  variation from MIS 4 to MIS 3 does not follow the %planktic pattern. Benthic foraminiferal diversity is generally low with Fisher  $\alpha$  values typically  $< 5$  and  $H(S) < 2$ . Peaks of  $H(S) (> 2)$  and Fisher  $\alpha (> 5)$  benthic diversity occur during the interglacial maxima of MIS 11, MIS 9e, MIS 8, MIS 7, MIS 5e, and MIS 1, where the assemblages are generally well preserved. Other peaks of diversity are present in MIS 6 and MIS 3 corresponding to maxima

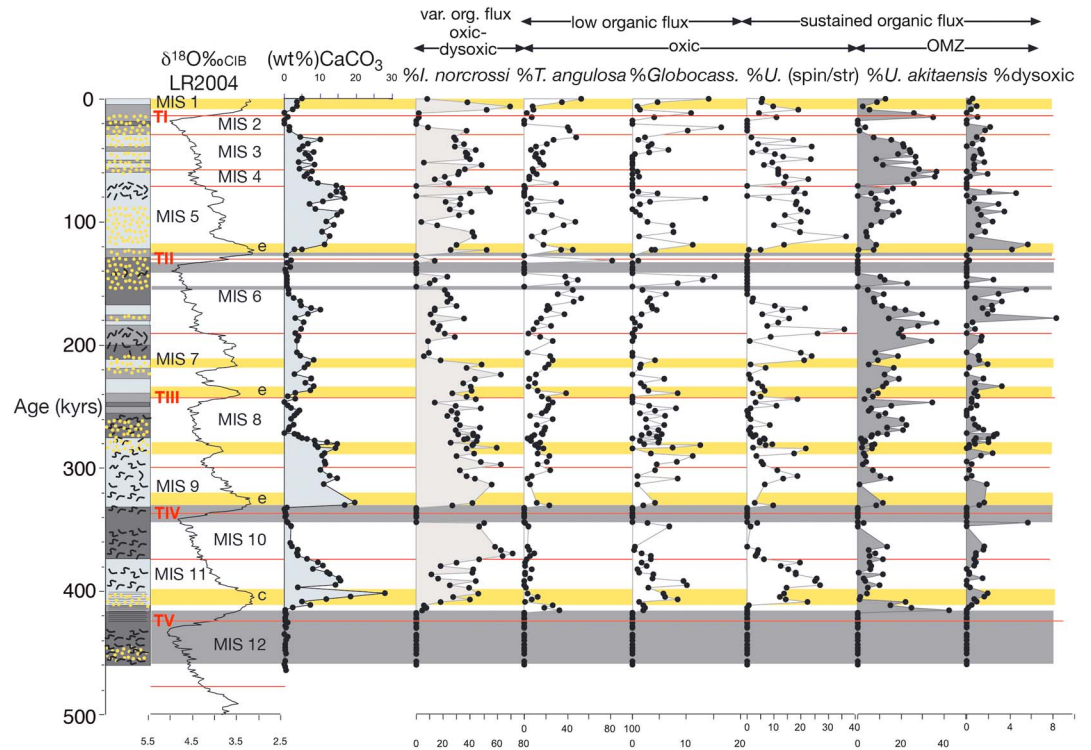


**Figure 7.** An age plot of common benthic species in the upper 460 kyrs of Site U1427. *I.* = *Islandiella*; *T.* = *Trifarina*; *Globocass.* = *Globocassidulina subglobosa*; *U.* = *Uvigerina*; spin/str = spinosa striate *Uvigerina* spp. Note: Var. org. flux = variable organic flux and OMZ = oxygen minimum zone. All benthic data in this figure are expressed as a percentage of total benthic calcareous foraminiferal data.

in foraminiferal concentration values. In general, the lowest diversity assemblages characterize glacial phases of MIS 10, MIS 8, MIS 6, and MIS 2 where the benthic fauna is not well preserved.

#### 4.3.1. Planktic Foraminifera

Three species of planktic foraminifera dominate (Figures 4 and 5): *Globigerina bulloides* (the thick-walled form of Domitsu & Oda, 2005, Figure 4a), *Neogloboquadrina pachyderma* sinistral (Figures 4d and 4e), and *Globigerina quinqueloba* (Figure 4c). Other common species include Tsushima Warm Current planktics (sensu Gallagher et al., 2015), *Globigerinoides ruber* and *Globorotalia tumida* (Figures 4h and 4i), *Pulleniatina obliquiloculata* (Figure 4j), *Neogloboquadrina incompta* (Figures 4f and 4g), and the colder water species *Globigerina umbilicata* (Figure 4j).

Prior to 180 ka *G. bulloides* are abundant at the base and top of MIS 11, near the top of MIS 10 and within MIS 8. *G. bulloides* abundance fluctuates markedly after 180 ka with maxima near the top of MIS 6 and during MIS 1. With the exception of MIS 4 *G. bulloides* are also common from MIS 5e to MIS 2. The abundance of *G. quinqueloba* is variable; this species is rare from MIS 11 to MIS 10 and MIS 5e to MIS 1 with maxima at ~180 and ~80 ka. *G. quinqueloba* is common between ~310 and 160 ka reaching a maximum from MIS 7 to MIS 6. *N. pachyderma* abundance in general shows the opposite pattern to the *G. bulloides* distribution (Figure 5), except in periods when TWC species dominate (especially *N. incompta*) at ~405 ka, 315 ka, and at present and where *G. quinqueloba* are most common. Although relatively rare, *G. umbilicata* peak in MIS 8 and MIS 6 and increase upward in abundance from MIS 3 to MIS 1.

#### 4.3.2. Benthic Foraminifera

Three calcareous foraminifera taxa dominate 50 to 90% of the benthic assemblages (Figures 6, 7): *Islandiella norcrossi* (Figure 6a), *Trifarina angulosa* (Figure 6b, also referred to as *Angulogerina ikebei*, Usami et al., 2013), and striate *Uvigerina* spp. The striate *Uvigerina* are also known as *U. akitaensis* (Figure 6e) and spinose-striate forms are equivalent to *U. cf. graciliformis*, (Figure 6d; cf. Fontanier et al., 2014). Other relatively common taxa include (Figure 6) *Cibicides* spp. (*C. pachyderma*, *C. refulgens*, and *C. lobatulus*; Figures 6h and 6j), *Elphidium*

**Table 2**  
The Environmental Distribution of Key Benthic Foraminifera Taxa in Figures 7 and 8

Benthic taxon	Oxygen level	Depth	Habitat	Comments
<i>Islandiella norcrossi</i>	suboxic-oxic	150–1,500 m	Shallow infauna	Moderate to high and seasonal surface productivity and organic matter flux in seasonally ice-free areas of northern high latitudes inhabit moderately organic (0.4–2.0%) sediment that shows opportunistic response on input of the phytodetritus in meso-oligotrophic areas
<i>Trifarina angulosa/ikebei</i>	suboxic-oxic	200–2,000 m	Shallow infauna	organic-poor (0.1–0.8%) coarse sediments and well-oxygenated bottom waters, low organic matter flux
<i>Globocassidulina subglobosa</i>	oxic	>200 m	Shallow infauna	found living above oxygen-depleted water masses (>45 mmol/L)
Striate spinose <i>Uvigerina</i> spp.	suboxic-oxic	200–1,000 m	Shallow infauna	
<i>Uvigerina</i> cf. <i>U. graciliformis</i> <i>Uvigerina akitaensis</i>	anoxic-dysoxic	200–1,000 m	Shallow infauna	high suspended particles and sustained organic matter flux inhabit a wide range of organic-enriched (0.3–5%) sediments, common in the OMZ on Japanese margin within oxygen-depleted water mass
<i>Globobulimina pacifica</i>	anoxic-dysoxic	200–1,000 m	Deep infaunal	OMZ, found living above oxygen-depleted water masses (>45 mmol/L)
<i>Glandulina laevigata</i>	anoxic-dysoxic	200–1,000 m	Deep infaunal	OMZ
<i>Brizalina</i> spp.	dysoxic	200–1,000 m	Shallow-intermediate infaunal	OMZ
<i>Fursenkoina bradyi</i>	anoxic-dysoxic	200–1,000 m	Deep infaunal	OMZ
<i>Cibicidoides pachyderma</i>	oxic	>100 m	Epifauna	
<i>Cibicidoides lobatulus</i>	oxic	0–200 m	Epifauna	
<i>Cibicidoides refulgens</i>	oxic	0–200 m	Epifauna	
<i>Elphidium excavatum</i>	oxic	0–100 m	Infaunal	
Millioliids ( <i>Quinqueloculina/Triloculina</i> spp.)	oxic	>0 m	Epifauna	
<i>Pullenia bulloides</i>	oxic	>200 m	Shallow infauna	well-oxygenated bottom and pore waters inhabit moderately organic-enriched (0.4–2.0%) sediments

Note. The main interpretations are from Bubenshchikova et al. (2008, 2015) and Fontanier et al. (2014). Other information is from references cited in text, especially Kaiho (1994) and Usami et al. (2013). OMZ = oxygen minimum zone.

spp. (especially *Elphidium excavatum*, Figures 6j and 6k), milioliids (*Quinqueloculina* spp. and *Triloculina* spp.), *Pullenia bulloides* (Figures 6l and 6m), and *Globocassidulina subglobosa* (Figure 6c).

*I. norcrossi* is the dominant species in the section making up >40–50% of the benthic rotaliid assemblage. It is most abundant from MIS 10 to the base of MIS 7 and rarest above this level in MIS 7, MIS 6, and MIS 2. *Uvigerina* spp. abundance fluctuate markedly. Spinose/striate *Uvigerina* spp. peak in MIS 11 with variable maxima and minima from MIS 9 to MIS 7 reaching a maximum at the base of MIS 6. The distribution of spinose/striate *Uvigerina* is highly variable from MIS 5e to MIS 1 with a minimum during MIS 2. *Uvigerina akitaensis* abundance is generally low; however, this taxon shows maxima at the base of MIS 11, top of MIS 8, base of MIS 6, and from MIS 4 to MIS 3.

The interval from the start of MIS 9 to the end of MIS 6 is characterized by short-lived peaks of less common benthic foraminiferal taxa. Taxa such as *Globobulimina pacifica* (Figure 6f) and *Fursenkoina bradyi* peak at ~170 ka, ~160 ka, and ~120 ka. Periodic maxima of neritic taxa (Figure 8) are present above interglacial maxima (MIS 9 to MIS 7) or just prior to glacial maxima (top of MIS 10 and MIS 6).

## 5. Discussion

### 5.1. Sedimentary Facies and Relative Sea Level

Sediment in the region near Site U1427 is dominated by sand facies shallower than 200-m water depth (the shelf edge), silt below 200 m, and clay below 500 m (Ohta et al., 2015). Assuming relative wave base has not

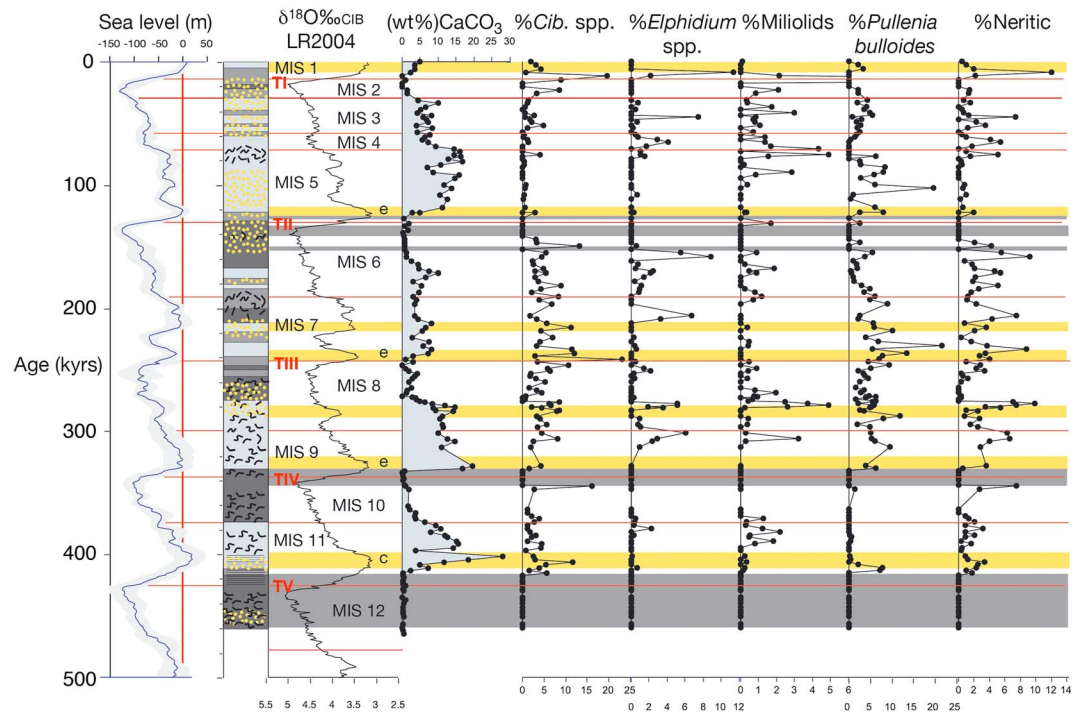


**Figure 8.** An age plot of common benthic taxa in the upper 460 kyrs of Site U1427 plotted with the sea level curve of Spratt and Lisiecki (2016). *Cib.* = *Cibicoides*. The benthic data for *Cibicoides*, *Elphidium*, *P. bulloides*, and %neritic taxa in this figure are expressed as a percentage of total calcareous benthic foraminiferal data (the list of taxa included in this column is in the text). The %Miliolids are expressed as a percentage of the total benthic fauna.

changed significantly in the last 460 kyrs, then glacial to interglacial sea levels are likely to have varied from ~337 (today's depth) to ~210 m (last glacial maximum depth; cf. Spratt & Lisiecki, 2016; Figure 6), accounting for the predominantly silty facies. These paleodepths are supported by the presence of generally high (> 50%) %planktic values in the sequence (Figure 3) typical of upper slope depths >200 m (van Hinsbergen et al., 2005). There is a strong relationship between facies and sea level. Calcareous silt dominated highstands. Clayey silt prevailed during the glacial maxima lowstands and silt during the terminations.

The clayey and sandy facies in lowstands reflect a closer proximity to the shelf edge and source of siliciclastics from regional fluvial systems, in the absence of inflow through the Tsushima Strait with the isolation of the Japan Sea (Tada, 2004). The lack of calcareous facies during these times may be due to a combination of dilution by siliciclastics (especially during periods with high sedimentation rates during Terminations V and IV and prior to TII, Figure 3) and/or decreased sea surface productivity (Tada et al., 1999, 2007). The predominance of clay (with high NGR values) during the glacials is likely related to eolian dust influx associated Chinese loess deposition (deMenocal et al., 1992). Intervals with increased Th/K and Th/U values in Site U1427 are interpreted to be related to increased aridity and dust influx (cf. Christensen et al., 2017; Groeneveld et al., 2017). Analyses of IODP 346 Site U1422 to the north of Site U1427 (Figure 1) showed that maxima in %K values in the Japan Sea are likely to be related to enhanced East Asian winter monsoon (EAWM) conditions and arid conditions over the last 3.6 million years (Zheng et al., 2018). The higher values of all these proxies at Site U1427 therefore reflect the generally drier stronger winter monsoonal conditions prevailed during glacial compared to interglacial periods (Figures 2 and 9). Silt deposition during the later stages of the glacial periods and the deglaciations is likely related to the rapid flooding of the Tsushima Strait causing increased inflow of ECSCW into the Japan Sea and increased seabed current activity. The lack of sandy facies during these times may relate to reduced fluvial activity due to arid conditions (cf. Dersch & Stein, 1994). The transition to highstand conditions during interglacials decreased clayey facies due to the increasing dominance of the ECSCW and/or the TWC higher-energy flow through the Tsushima Strait. Similar warm sea surface temperatures to today, due to TWC inflow, increased marine carbonate

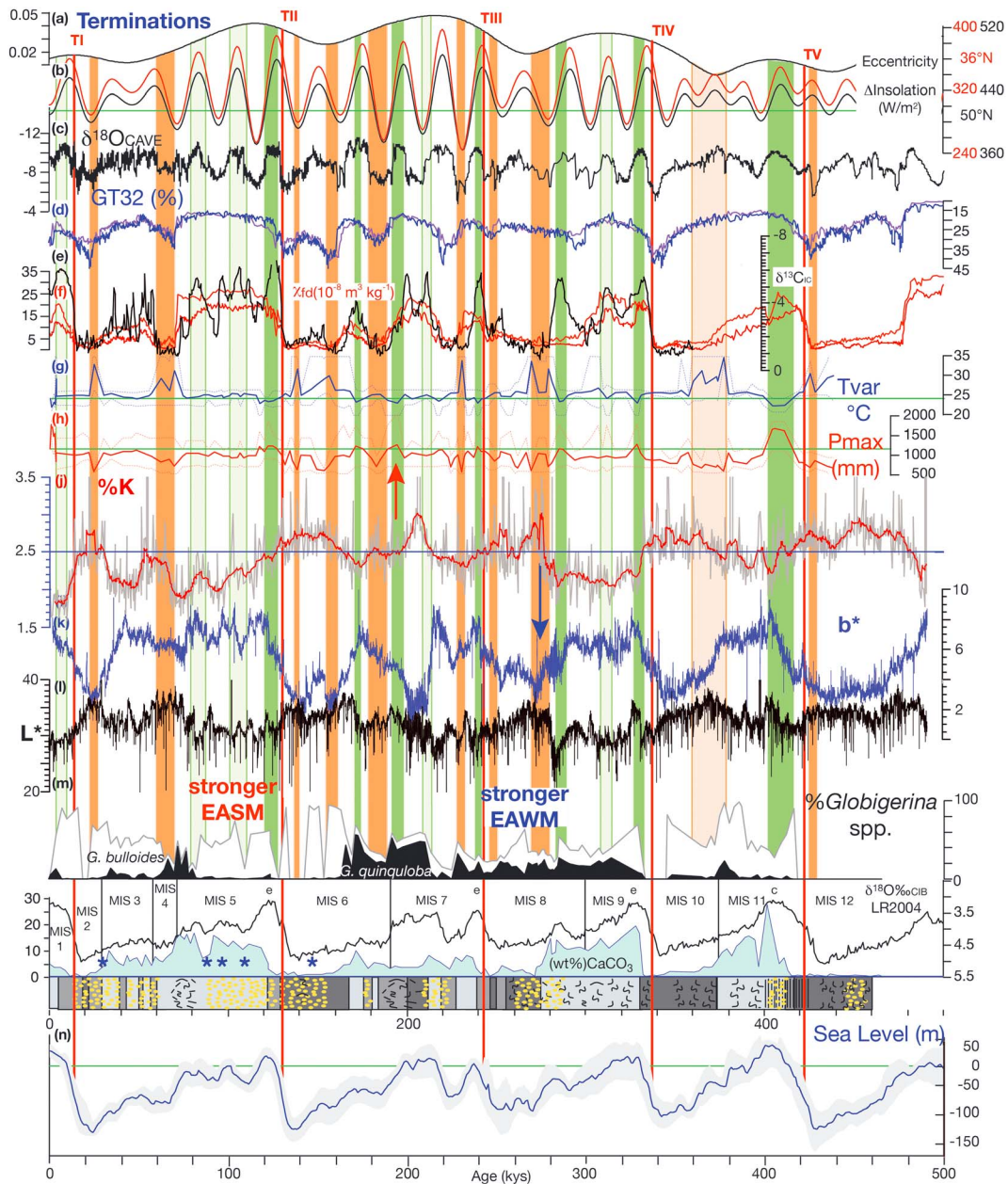


**Figure 9.** The relationship between the stratigraphy of Site U1427 and (a) eccentricity and (b) insolation in watts per square meter (at 36°N and 50°N) created using Analyseries 2.0.4 software (Paillard et al., 1996) and the Laskar et al. (2004) solution; (c) the Chinese stalagmite record of the Asian monsoon (Cheng et al., 2016); (d and f) Chinese loess record of GT32% (%32-mm particle content) and frequency-dependent magnetic susceptibility data from the Yimaguan and Louchuan sections (Hao et al., 2012); (e) the carbon isotope values of inorganic carbonates of Chinese loess is shown in per mill (Sun et al., 2015). (g and h) Temperature and precipitation variability at Lake Biwa inferred from palynological data, the green horizontal lines are modern values (Nakagawa et al., 2008). Tvar°C denotes the temperature difference between winter and summer, whereas Pmax is the maximum estimated precipitation. When Pmax is elevated and Tvar reduced strong summer monsoonal conditions are interpreted (Nakagawa et al., 2008), the pattern reverses a stronger winter monsoon prevailed; (m) the LR2004 stack (Lisiecki & Raymo, 2005), the asterisks are horizons of ice-rafted debris documented by Ikehara and Itaki (2007) in the northern part of the Japan Sea. The colored vertical bars denote where proxies suggest enhanced EASM (green, red arrow) and stronger EAWM (orange, blue arrow). We have annotated periods with stronger EAWM and EASM by darker colors, as these are time when the majority of the patterns of the proxies align. The lighter shade is weaker yet distinct EAWM and EASM periods. Note: The location of the proxy records above is in Figure 1. The %K, brightness (L\*), and b\* for Site U1427 is plotted in age, also showing percentage of *Globigerina* spp. in the total planktic assemblage. The black curve is %*Globigerina quinqueloba*, the remaining species (white) are primarily *Globigerina bulloides* with minor *Globigerina umbilicata*. The lowermost curve are global sea level estimates with error ranges (Spratt & Lisiecki, 2016). EAWM = East Asian winter monsoon; EASM = East Asian summer monsoon.

(calcareous microfossil) productivity during the highest sea level periods depositing calcareous silt. The sand and occasional maxima in neritic microfossils in highstand calcareous facies may have been transported via downslope mass wasting from the edge of the shelf and possibly via a *submarine valley/canyon* nearby (Ohta et al., 2015).

### 5.2. Sea Surface Conditions

Modern planktic foraminiferal assemblages reflect sea surface temperature and relative nutrient conditions in the Japan Sea (Domitsu & Oda, 2005; Kuroyanagi & Kawahata, 2004). The assemblages are dominated by warmer water *N. incompta* (<20 °C, Tsushima waters and high chlorophyll- $\alpha$  concentrations; Kuroyanagi & Kawahata, 2004) and colder water *N. pachyderma* (<12 °C, typically ~5 °C) with lesser amounts of *G. bulloides* and *G. quinqueloba*, taxa with wide temperature tolerances (Bé & Hutson, 1977; Kuroyanagi & Kawahata, 2004). Presently, *G. bulloides* (thick-walled form) and *G. quinqueloba* are abundant in nutrient-rich low-salinity water in the Tsushima Strait (Domitsu & Oda, 2005) associated with an inflow of freshwater (ECSCW) from the Yangtze River. *G. quinqueloba* is also common in sediment of the coastal region of western Japan associated with fluvial freshwater input (Domitsu & Oda, 2005). *G. quinqueloba* shows a strong correlation to high chlorophyll- $\alpha$  concentrations, and *G. bulloides* (thin-walled) is associated with upwelling in the Japan Sea near the Tsugaru and Tsushima Straits (Kuroyanagi & Kawahata, 2004). The modern distribution of *G. umbilicata* is not well known as it is rare in the Japan Sea; however, it is typical of cold low-salinity last glacial maximum water in the region (Ujiié et al., 1983).

Previous analyses of glacial/interglacial planktic foraminiferal distribution (Domitsu & Oda, 2005; Ortakand et al., 2015; Usami et al., 2013) indicate that the present assemblage distribution typifies only brief interglacial warmer TWC anomalies in the predominantly cold oceanic conditions in the Japan Sea over the last 160 kyrs. The high concentration of subpolar to polar *N. pachyderma* at Site U1427 suggests that cold (<12 °C, ~5 °C average) oceanic conditions prevailed in all but the glacial/interglacial maxima over the last 460 kyrs.

The presence of abundant *G. bulloides* (with rarer *G. umbilicata*) during glacial maxima MIS 2, MIS 6, and MIS 10 (Figure 5) suggest cold lower salinity nutrient-rich surface water conditions. A similar assemblage in core MD01-2407 to the north of Site U1427 is interpreted to represent the mixing of high nutrient surface water caused by enhanced winter cooling due to the intensification of the winter monsoon (Usami et al., 2013). Alternatively, *G. bulloides* (thick-walled) incursions during MIS 5, MIS 8, MIS 9, and MIS 11 and Terminations TV, TIV, TII, and TI are likely to be related to the inflow of fresh water and nutrients from the China Sea (ECSCW) via the Tsushima Strait during summer monsoon conditions.

Maxima of *G. quinqueloba* may also be related to fresh water inflow from the China Sea (possibly during summer monsoon conditions during MIS 11); however, their abundance in other intervals is most likely to be related to proximal fluvial runoff from the adjacent Japanese coastal region during the winter and/or summer monsoon. The switch from *G. bulloides* dominance (MIS 11/MIS 10) to upward increasing *G. quinqueloba* from MIS 9 to MIS 6 suggests a marked increase in chlorophyll- $\alpha$  in the surface waters. The planktic assemblage from MIS 9 to MIS 6 is similar to the modern biota from the coastal region off western Japan (Domitsu & Oda, 2005), suggesting increased proximal fluvial freshwater influence on the salinity variability in the absence of ECSCW input. The *G. quinqueloba* maximum from MIS 5 to MIS 4 is interpreted to reflect Japan Sea Coastal Water (JSCW) input.

Brief incursions of surface water dwelling subtropical oligotrophic *G. ruber* (Peeters et al., 2002) and the warmer water deeper dwelling *N. incompta* (associated with high chlorophyll- $\alpha$  concentrations; Kuroyanagi & Kawahata, 2004) signify modern TWC conditions prevailed during MIS 1, MIS 5e, and MIS 9, and in particular during the exceptionally warm interglacial period MIS 11 (Droxler et al., 2003). Other intervals lack faunal evidence for strong TWC influence, suggesting that optimal conditions for this current to reach the Japan Sea were only facilitated by the highest interglacial sea levels in the Tsushima Strait. In contrast, the lack of any fauna (planktic or benthic) during glacial maxima MIS 12 and MIS 10, and intermittently during MIS 6, suggests periods of reduced oceanic productivity during the lowest sea levels (see section below).

### 5.3. Sea Bed Conditions

The majority of the benthic foraminiferal assemblages in U1427 are less diverse than other shelf regions and deep ocean environments worldwide (where  $H(S) \gg 5$  and Fisher  $\alpha \gg 5$ ; Murray, 2006). The diversity values are comparable to more restricted environments such as normal marine estuary or lagoonal settings (Murray,

2006). Overall, the relatively low assemblage diversity is likely related to the high latitude and restricted nature of the Japan Sea. Nevertheless, diversity maxima during the warmest interglacial phases show that more open marine shelf/deep sea environments prevailed during sea level highstands. Conversely, very low diversity values signify periods when the Japan Sea was restricted during sea level lowstands. The dominant benthic foraminifera at Site U1427 (Figures 6 and 7) are also common in the Japan and the Okhotsk Sea (Usami et al., 2013; Bubenshchikova et al., 2008, 2015; Table 2). *I. norcrossi* are found at depths from 150 to 1500 m in suboxic to oxic organic-rich sediment with moderate to high seasonal surface productivity and relatively high stable sea bed salinity (Bubenshchikova et al., 2015; Hasegawa, 1979; Inoue, 1989; Usami et al., 2013). *T. angulosa* are present from 200 to 2000 m in suboxic to oxic conditions in organic poor sediments (Bubenshchikova et al., 2008, 2015; Hasegawa, 1979; Inoue, 1989; Ujiie et al., 1983; Usami et al., 2013; Table 2). *Uvigerina* spp. typically are associated with sustained organic flux and/or dysoxic conditions at the seafloor and within the uppermost few centimeters of the sediment (Jorissen et al., 1995, 2007; Jorissen, 1999). *U. akitaensis* inhabits organic-rich sediments associated with high surface productivity and dysoxic to anoxic conditions (Bubenshchikova et al., 2015; Fontanier et al., 2014; Table 2) at depths greater than 200 m in the Japan Sea (Hasegawa, 1979; Matoba & Fukasawa, 1992). Spinose-striate *Uvigerina* species such as *U. cf. graciliformis* inhabit slightly more oxic conditions with a lower organic flux than *U. akitaensis* (Bubenshchikova et al., 2008, 2015; Fontanier et al., 2014) at depths greater than 100 m (Ujiie et al., 1983). *G. subglobosa*, *Cibicidoides pachyderma*, and *P. bulloides* are cosmopolitan taxa common in oxic conditions associated with low surface productivity and strong bottom currents (Poli et al., 2012) at depths greater than 200 m (Hasegawa, 1979; van Hinsbergen et al., 2005). Taxa typical of dysoxic conditions (sensu Fontanier et al., 2014 and Kaiho, 1994) are rare and include (Figures 6 and 7 and Table 2) *Brizalina* spp., *Glandulina laevigata* (Figure 6g), *F. bradyi*, and *G. pacifica* (Figure 6f). Neritic species of the miliolids *Quinqueloculina* spp., *Triloculinella* spp., *Elphidium* spp., *Cibicidoides lobatulus*, and *C. refulgens* (Akimoto & Hasegawa, 1989; Hasegawa, 1979; van Hinsbergen et al., 2005) are typically oxic taxa (Kaiho, 1994). Overall, the dominant benthic assemblages at Site U1427 suggest that site remained bathed in suboxic to oxic conditions above the dysoxic zone (Tada et al., 2007) for most of the last 460 kyrs. However, there were considerable variations in nutrient flux and intervals with lower oxygen conditions.

The minimal low diversity benthic fauna (with less than five benthic foraminifera/g sediment, Figure 3), absence of bioturbation, and presence of laminations suggest periodic oxygen minimum zone (OMZ) conditions and/or reduced oceanic productivity during glacial maxima. Some of these horizons (MIS 8, MIS 6, and MIS 2) are equivalent to the glacial maxima dark layers deposited in the deeper water core MD01-2407 north of Site U1427 (Figure 1), reflecting stratified shallow (<237-m paleodepth) low oxygen events across the Japan Sea (Kido et al., 2007; Tada, 1994; Tada et al., 2018; Usami et al., 2013; Watanabe et al., 2007). Similar to Okhotsk Sea (Bubenshchikova et al., 2015), reduced oxygen and stratified oceanic conditions prevailed during Terminations TV, TIII, TII, and TI. These conditions weakened in the later stages of each deglaciation and became much weaker during interglacial periods representing the well-mixed aerobic interglacial mode of the Japan Sea (Tada, 1994; Usami et al., 2013; Watanabe et al., 2007). Intense fluctuating OMZ conditions during MIS 7–MIS 6 and MIS 4–MIS 3 were followed by oxic and low organic flux conditions (MIS 6 and MIS 3/2) suggesting that enhanced oceanic mixing and oxygenation typified the onset of glacial conditions. The presence of increased neritic taxa during MIS 10 and MIS 6 (Figure 8) may be related to the proximity of the shelf during glacial maxima and possibly transported downslope. Peaks in neritic taxa during TI, MIS 9, and MIS 7 may also represent increased downslope transportation of foraminiferal tests due to highstand upper slope instability and/or increased oceanic current activity with the rapid flooding of the Tsushima Strait. The neritic maxima in MIS 8, late MIS 7/MIS 6, and MIS 4/MIS 3 may relate to downslope sediment transport due to falling sea level.

## 6. East Asian Monsoon Variability Over the Last 460 Kyrs

### 6.1. Chinese Loess, Cave, and Lake Biwa Records

Asian monsoon variability is modulated by precession (~23 ky) and/or obliquity (~41 ky) insolation (Figure 9; Cheng et al., 2016; Nakagawa et al., 2008; Sun et al., 2015) when stronger winter monsoon conditions are interpreted to have prevailed during glacial periods (Zheng et al., 2018) and an enhanced summer monsoon during interglacial maxima (Fujine et al., 2009; Usami et al., 2013). In the Japan Sea, freshwater discharge from the Yangtze River via the Tsushima Strait lowers the salinity and increases the nutrient flux of the Japan Sea

during enhanced summer monsoon conditions in MIS 1 and MIS 5 (Tada, 2004). In contrast, enhanced ventilation and sea ice (ice rafted debris in the northern part of the Japan Sea, the asterisks in Figure 9) typically occur in the Japan Sea during the winter monsoon conditions during glacial maxima and occasionally during MIS 5 (Ikehara & Itaki, 2007; Tada, 2004).

We extend the 160-kyr record of MD01-2407 (Figure 1) to 460 kyrs and compare our data (Figure 9) with Japanese Lake Biwa palynological (Nakagawa et al., 2008), Chinese speleothem (Cheng et al., 2016), and Chinese loess (Hao et al., 2012; Sun et al., 2015) data. The lightest cave oxygen and loess carbon isotope values are interpreted to typify periods of EASM intensification (the dark green vertical bars; Figure 9) associated with the lowest temperature variability and highest precipitation estimates in Lake Biwa. The concurrent patterns in these proxies suggest that the strongest EASM conditions prevailed across the region following Terminations TV to TII, during MIS 8/MIS 7e interglacial warm periods (Figure 9) and with the exception of MIS 11e prevailed during the transition from insolation maxima to minima. A weaker EASM is interpreted during interglacial maxima in MIS 9, MIS 5, and MIS 1 (light green vertical bars; Figure 9) in the Chinese loess and speleothem records associated with insolation maxima, when floral proxies at Lake Biwa do not show a strong temperature or precipitation signal. These differences suggest a variable East summer monsoon strength, which may reflect latitudinal switches in the monsoon front from Japan to China. More intense EAWM conditions are interpreted during periods when relatively more enriched cave oxygen and loess carbon isotope values coincide with highest temperature variability and lowest rainfall estimates at Lake Biwa (dark orange vertical bars; Figure 9). These coincide with transitions from low to high insolation or insolation minima in MIS 8, MIS 6, MIS 4, and MIS 2 (Figure 10). The cave and loess signals for the EAWM are not as strong during periods of low insolation variability from MIS 11 to MIS 10, coinciding with a period of relative low precipitation and high temperature variability in Lake Biwa (light orange vertical bars; Figure 9).

## 6.2. The Japan Sea Record of the Asian Monsoon

At Site U1427 patterns in the  $b^*$  (related to %carbonate) and  $L^*$  (brightness) that reflect TOC (cf. Sagawa et al., 2018) are partially controlled by sea level variability (Figure 9), where reduced  $b^*$  and increased  $L^*$  typifying glacial maxima, whereas increased  $b^*$  and lower  $L^*$  prevail in interglacials. However, the lithological characteristics at Site U1427 are related to East Asian Monsoon intensity. For example, higher %K (cf. Zheng et al., 2018), lighter ( $L^*$ ) silts, and clayey silts with lower  $b^*$  values coincide with periods of more intense EAWM (MIS 10, MIS 8, MIS 6, MIS 4, and MIS 2; Figures 9 and 10) conditions, whereas generally lower %K, darker ( $L^*$ ), and relatively high  $b^*$  silts were deposited during times of increased EASM (MIS 11c, MIS 9e, start of MIS 8, MIS 7e, start of MIS 6, and MIS 5e; Figures 9 and 10). The terminations corresponds to the transitions between enhanced winter and summer monsoon conditions (Figure 10). In addition to insolation forcing the monsoonal patterns in Figure 9 also reflect glacial/interglacial (ice volume, CO<sub>2</sub>) forcing of the monsoonal system (Cheng et al., 2016; Sun et al., 2015). One to two periods of the strongest East Asian winter monsoon (EAWM) prevail in glacial phases (with an enhanced Northern Hemisphere ice sheet), whereas up to three periods of enhanced EASM typify interglacial phases (during glacial retreat). The latitudinal variability in the intensity of the EASM and EAWM between the Chinese and Japanese monsoon records (the light orange and green intervals) also reflects variations in thermal contrast between land (Asian continent) and sea (Japan) and an overall latitudinal thermal gradient (Sun et al., 2015). The matches and mismatches in patterns between these multiproxy records suggest that a complex interplay between ice sheet dynamics, insolation, and thermal gradient controls the nature and intensity of the East Asian monsoon.

Over the last 460 kyrs, nutrient flux, salinity, and relative oxygenation have varied markedly (Figures 9 and 10) at Site U1427. Much of this variability is related to sea level fluctuations during glacial maxima, such as dysoxia and low oceanic productivity causing foraminiferal faunal minima during MIS 12, MIS 10, MIS 6, and MIS 2, with TWC planktic assemblage and diverse benthic foraminiferal influxes during interglacial maxima. However, planktic foraminiferal assemblage variability also seems to be modulated by the relative intensity of the East Asian winter and summer monsoons.

The distribution of the common planktic species *G. bulloides* and *G. quinqueloba* at Site U1427 is related to salinity (relative influence of ECSCW and JSCW) and sea surface nutrient flux. Peaks of these taxa commonly coincide with enhanced monsoonal conditions (Figure 9), suggesting regular surface plankton blooms particularly during the EASM. Similar patterns in the relative abundance *G. bulloides* are used as upwelling and

(a) MIS 2, 4, 6, 8, 10  
low → high insolation  
& insolation minima

(b) Terminations I, II, IV, V

(c) MIS 5e, 7e, 9e, 11c\*  
high → low insolation  
transitions

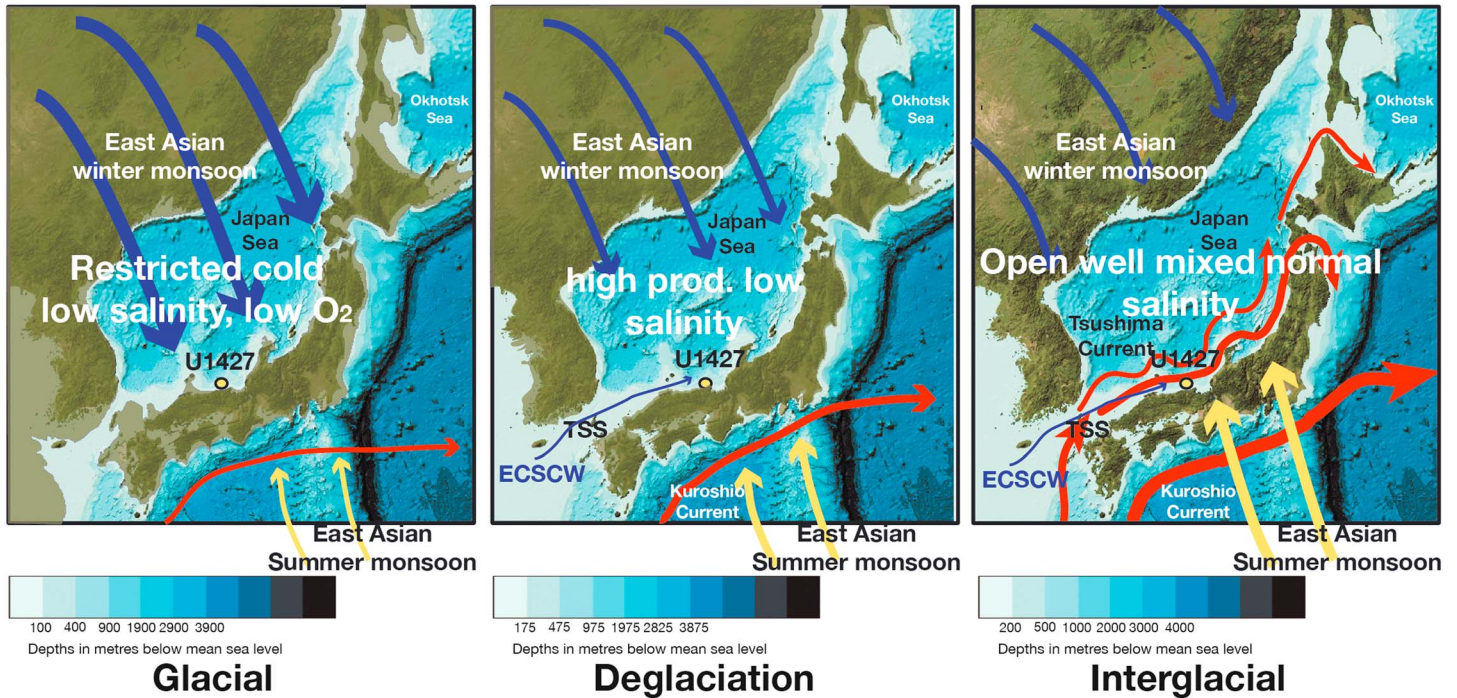


**Figure 10.** Variations in oceanography and the position and intensity of the East Asian monsoon during (a) low to high insolation transitions and insolation minima, (b) terminations, and (c) high to low insolation transitions. \*MIS 11c coincides with an insolation maxima during an eccentricity low (Figure 9). The thicker blue arrows signify enhanced EAWM and thicker yellow arrows a stronger EASM. The thin blue line (ECSCW) is the path of fresh water from the China Sea during terminations and interglacial maxima. The temporal variations in the Kuroshio current position and strength are adapted from Gallagher et al. (2015). The base map is from General Bathymetric Chart of the Oceans ([www.gebco.net](http://www.gebco.net)) where modern bathymetry represents interglacial maxima (see also Figure 1). This is recalibrated to ~100 m below present for glacial phases and ~25 m below present during the terminations. The paleoshorelines during these sea level phases are adapted from Hayashi et al. (2017). Prod. = productivity; ECSCW = East China Sea Coastal Water; EAWM = East Asian winter monsoon; MIS = marine isotope stage.

nutrient flux indicators signifying Indian monsoon intensification in the Arabian Sea (Kroon et al., 1991). *G. bulloides* maxima occur in MIS 11, MIS 9/MIS 8 (part), and MIS 5 due to increased fresh water influx from the East China Sea (EACSW) during enhanced EASM conditions when sea levels were high enough to breach the Tsushima Strait. However, when this strait was restricted by lower sea level (during MIS 8, MIS 7, and MIS 6) maxima of *G. quinqueloba* reflect fresh water influx from Japan (JSCW) during the EASM (Figure 8). The pattern of peaks of *Globigerina* spp. during the winter monsoon is not as distinct as the summer, occasionally maxima coincide with enhanced EAWM during MIS 10, MIS 7, MIS 6, and MIS 2.

## 7. Conclusions

The semi-enclosed Japan Sea is an ideal region to investigate the interaction between the ocean, climate, and sea level variability. The typical interglacial/glacial mode for the deep water (>1,000 m) Japan Sea is well documented for the last ~160 kyrs (Tada et al., 1999; Usami et al., 2013) where freshwater discharge from the Yangtze River via the Tsushima Strait lowered the salinity and increased the nutrient flux of the Japan Sea during the summer monsoon in MIS 1 and MIS 5. Enhanced ventilation and northern sea ice (ice-rafted debris) occurred in the Japan Sea in winter monsoon conditions during glacial maxima and MIS 5. Foraminiferal and sediment facies analyses from the relatively shallow (325-m depth) IODP Expedition 346 Site U1427 in the Japan Sea reveal a ~460-kyr record of highly variable nutrient flux and sea bottom ventilation that is related to relative sea level variability, the depth of the Tsushima Strait, and East Asian monsoon intensity.

At this shallow site, sea level variations have a large impact on processes and the origin of sedimentary facies and biofacies. Calcareous silt dominates interglacials when depths were either higher than or 50 m below present. Clayey silt prevails in glacial maxima and silt during terminations. The lack of calcareous facies during glacial maxima may have been caused by dilution by siliciclastic sediment input and/or reduced oceanic surface productivity. Silt deposition during terminations is likely related to the rapid flooding of the Tsushima Strait causing increased inflow of ECSCW into the Japan Sea and increased current activity.

Previous analyses of glacial/interglacial planktic foraminiferal distribution suggest that modern assemblages typify interglacial warmer TWC *anomalies* in the predominantly cold Japan Sea over the last 160 ka. At Site U1427 brief incursions of surface water dwelling subtropical oligotrophic *G. ruber* and the warmer water deeper dwelling *N. incompta* suggest “modern” TWC conditions prevailed during MIS 1, MIS 5e, and MIS 9 and were especially strong during MIS 11. Other intervals lack TWC planktic foraminifera, suggesting that optimal conditions for this current to reach the Japan Sea were only facilitated by the highest interglacial sea levels in the Tsushima Strait. The subpolar to polar *N. pachyderma* is the most common planktic species in the section suggesting that cold (~5 °C average) oceanic conditions prevailed in all but the glacial/interglacial maxima over the last 460 kyrs.

The lack of planktic and benthic foraminifera, absence of bioturbation, and presence of laminations suggest periodic reduced oxygen conditions during many glacial maxima, suggesting enhanced oceanic stratification during some periods of lowest sea level (cf. Tada et al., 2007). Similar to Okhotsk Sea (Bubenshchikova et al., 2015) stratified lower oxygen conditions characterize Terminations TV, TIII, TII, and TI (Figure 10). These conditions weakened during interglacial periods when the Japan Sea transitioned to a well-mixed aerobic interglacial *mode* (Figure 10; Tada, 1994; Usami et al., 2013; Watanabe et al., 2007). Fluctuating OMZ conditions followed by oxic low organic flux conditions during the onset of glacial periods suggest that enhanced oceanic mixing and oxygenation were associated with the isolation of the Japan Sea during the lowest sea levels.

While the facies and foraminiferal variability at Site U1427 are controlled by relative sea level, the biofacies patterns also reflect East Asian monsoon variability. The middle to late Pleistocene history of the East Asian winter and summer monsoons has been interpreted from palynofloral records in Lake Biwa, Japan (Nakagawa et al., 2008), Chinese speleothem (Cheng et al., 2016), and loess (Hao et al., 2012; Sun et al., 2015) data (Figure 9). The lightest cave oxygen and loess carbon isotope values typify EASM intensification with the lowest temperature variability and highest precipitation at Lake Biwa. These data suggest enhanced East Asian monsoon conditions following Terminations TV to TII, during MIS 8/MIS 7 that prevailed during the transition from insolation maxima to minima. Intense EAWM conditions coincide with transitions from low to high insolation or insolation minima in MIS 8, MIS 7, MIS 6, MIS 4, and MIS 2. When compared to foraminiferal and sedimentary facies data at Site U1427 (Figure 9) patterns, the lighter silts and clayey silts with lower %carbonate values coincide with periods of more intense EAWM during MIS 8, MIS 6, MIS 4, and MIS 2 (Figure 10). In contrast, the darker calcareous silts were deposited during times of increased EASM during MIS 11c, MIS 9e, MIS 8, MIS 7e, MIS 6, and MIS 5e (Figure 10). Peaks of *G. bulloides* and *G. quinqueloba* commonly coincide with enhanced monsoonal conditions (Figure 9), suggesting regular surface plankton nutrient enrichment and influx of fresh water from the East China Sea during the EASM when sea levels were high enough to breach the Tsushima Strait. However, when the Tsushima Strait was restricted by lower sea level, maxima of *G. quinqueloba* reflect a switch to a Japanese source of fresh water influx from Japan during the summer monsoon.

Insolation forcing is a strong control on the monsoonal intensity in loess, cave, and lake records in the region. However, the fact that the strongest EAWM events prevail in glacial phases whereas several enhanced EASM periods typify interglacial phases suggests glacial/interglacial (ice volume, CO<sub>2</sub>) forcing of the monsoonal system. Apparent mismatches between the Chinese and Japanese East Asian monsoonal intensity between proxies suggest that latitudinal and land/sea thermal contrasts also have roles to play in East Asian monsoon variability. This suggests that a complex interplay between ice sheet dynamics, insolation, and thermal gradient controls the nature and intensity of the East Asian monsoon.

## References

- Akimoto, K., & Hasegawa, S. (1989). Bathymetric distribution of the recent benthic foraminifers around Japan—As a contribution to the new paleobathymetric scale. *Memory of Geological Society of Japan*, 32, 229–240.
- Aoki, K. (2008). Revised age and distribution of ca. 87 ka Aso-4 tephra based on new evidence from the Northwest Pacific Ocean. *Quaternary International*, 178(1), 100–118. <https://doi.org/10.1016/j.quaint.2007.02.005>

## Acknowledgments

This research used samples and data provided by the Integrated Ocean Drilling Program. We thank the IODP-U.S. Implementing Organization staff and the SIEM Offshore crew for their invaluable assistance and skill during Expedition 346. Funding was provided by the Australian IODP Office and the ARC Basins Genesis Hub (IH130200012) to S. J. G. This is also part of a DAAD collaboration between S. J. G. and D. D. V. We thank the Editor (Ellen Thomas) and two anonymous reviewers for their thorough constructive feedback that improved the text. The microfossil data used in this paper are included in AGU Paleoceanography supporting information Data Sets S1 and S2.

- Bé, A. W., & Hutson, W. H. (1977). Ecology of planktonic foraminifera and biogeographic patterns of life and fossil assemblages in the Indian Ocean. *Micropaleontology*, 23(4), 369–414. <https://doi.org/10.2307/1485406>
- Bubenschikova, N., Nürnberg, D., Lembke-Jene, L., & Pavlova, G. (2008). Living benthic foraminifera of the Okhotsk Sea, faunal composition, standing stocks and microhabitats. *Marine Micropaleontology*, 69(3–4), 314–333. <https://doi.org/10.1016/j.marmicro.2008.09.002>
- Bubenschikova, N., Nürnberg, D., & Tiedemann, R. (2015). Variations of Okhotsk Sea oxygen minimum zone: Comparison of foraminiferal and sedimentological records for latest MIS 12–11c and latest MIS 2–1. *Marine Micropaleontology*, 121, 52–69. <https://doi.org/10.1016/j.marmicro.2015.09.004>
- Cheng, H., Edwards, R. L., Sinha, A., Spötl, C., Yi, L., Chen, S., et al. (2016). The Asian monsoon over the past 640,000 years and ice age terminations. *Nature*, 534(7609), 640–646. <https://doi.org/10.1038/nature18591>
- Christensen, B. A., Renema, W., Henderiks, J., De Vleeschouwer, D., Groeneveld, J., Castañeda, I., et al. (2017). Indonesian throughflow drove Australian climate from humid Pliocene to arid Pleistocene. *Geophysical Research Letters*, 44, 6914–6925. <https://doi.org/10.1002/2017GL072977>
- De Vleeschouwer, D., Dunlea, A. G., Auer, G., Anderson, C. H., Brumsack, H., de Loach, A., et al. (2017). Quantifying K, U, and Th contents of marine sediments using shipboard natural gamma radiation measured on DV JOIDES resolution. *Geochemistry, Geophysics, Geosystems*, 18, 1053–1064. <https://doi.org/10.1002/2016GC006715>
- deMenocal, P. B., Bristow, J. F., & Stein, R. (1992). Paleoclimate applications of downhole logs: Pliocene-Pleistocene results from Hole 798B, Sea of Japan. In *Proceedings of the Ocean Drilling Program, Scientific Results, Vol. 127/128, Pt. 1*
- Dersch, M., & Stein, R. (1994). Late Cenozoic records of eolian quartz flux in the Sea of Japan (ODP leg 128, sites 798 and 799) and paleoclimate in Asia. *Palaeogeography, Palaeoclimatology, Palaeoecology*, 108(3–4), 523–535. [https://doi.org/10.1016/0031-0182\(94\)90250-X](https://doi.org/10.1016/0031-0182(94)90250-X)
- Domitsu, H., & Oda, M. (2005). Japan Sea planktic foraminifera in surface sediments: Geographical distribution and relationships to surface water mass. *Paleontological Research*, 9(3), 255–270. <https://doi.org/10.2517/prpsj.9.255>
- Droxler, A. W., Alley, R. B., Howard, W. R., Poore, R. Z., & Burckle, L. H. (2003). Unique and exceptionally long interglacial marine isotope stage 11: Window into Earth warm future climate. In A. W. Droxler, R. Z. Poore, & L. H. Burckle (Eds.), *Earth's Climate and Orbital Eccentricity: The marine isotope stage 11 Question* (p. 14). Washington, DC: American Geophysical Union. <https://doi.org/10.1029/137GM01>
- Fontanier, C., Duros, P., Toyofuku, T., Oguri, K., Koho, K. A., Buscail, R., et al. (2014). Living (stained) deep-sea foraminifera off Hachinohe (NE Japan, western Pacific): Environmental interplay in oxygen-depleted ecosystems. *Journal of Foraminiferal Research*, 44(3), 281–299. <https://doi.org/10.2113/gsjfr.44.3.281>
- Fujine, K., Tada, R., & Yamamoto, M. (2009). Paleotemperature response to monsoon activity in the Japan Sea during the last 160 kyr. *Palaeogeography, Palaeoclimatology, Palaeoecology*, 280(3–4), 350–360. <https://doi.org/10.1016/j.palaeo.2009.06.022>
- Gallagher, S. J., Kitamura, A., Iryu, Y., Itaki, T., Koizumi, I., & Hoiles, P. W. (2015). The Pliocene to recent history of the Kuroshio and Tsushima warm currents: A multi-proxy approach. *Progress in Earth and Planetary Science*, 2(1), 1–17. <https://doi.org/10.1186/s40645-015-0045-6>
- Gallagher, S. J., Wallace, M. W., Li, C. L., Kinna, B., Bye, J. T., Akimoto, K., & Torii, M. (2009). Neogene history of the West Pacific warm pool, Kuroshio and Leeuwin currents. *Paleoceanography*, 24, PA1206. <https://doi.org/10.1029/2008PA001660>
- Gamo, T., & Horibe, Y. (1983). Abyssal circulation in the Japan Sea. *Journal of the Oceanographical Society of Japan*, 39(5), 220–230. <https://doi.org/10.1007/BF02070392>
- Gooday, A. J. (2003). Benthic foraminifera (protista) as tools in deep-water palaeoceanography: Environmental influences on faunal characteristics. In A. J. Southward, P. A. Tyler, C. M. Young, & L. A. Fuiman (Eds.), *Advances in marine biology*, (Vol. 46, pp. 3–90). London, UK: Academic Press.
- Groeneveld, J., Henderiks, J., Renema, W., McHugh, C. M., De Vleeschouwer, D., Christensen, B. A., et al. (2017). Australian shelf sediments reveal shifts in Miocene Southern Hemisphere westerlies. *Science Advances*, 3, e1602567.
- Hao, Q., Wang, L., Oldfield, F., Peng, S., Qin, L., Song, Y., et al. (2012). Delayed build-up of Arctic ice sheets during 400,000-year minima in insolation variability. *Nature*, 490(7420), 393–396. <https://doi.org/10.1038/nature11493>
- Hasegawa, S. (1979). Foraminifera of the Himi Group, Hokuiku Province Central Japan, Tohoku University scientific report 2nd series (*Geology*), 49, 89–181.
- Hayashi, R., Takahara, H., Inouchi, Y., Takemura, K., & Igarashi, Y. (2017). Vegetation and endemic tree response to orbital-scale climate changes in the Japanese archipelago during the last glacial–interglacial cycle based on pollen records from Lake Biwa, western Japan. *Review of Palaeobotany and Palynology*, 241, 85–97. <https://doi.org/10.1016/j.revpalbo.2017.02.008>
- Hoiles, P. W., Gallagher, S. J., Kitamura, A., & Southwood, J. M. (2012). The evolution of the Tsushima current during the early Pleistocene in the Sea of Japan: An example from marine isotope stage (MIS) 47. *Global and Planetary Change*, 92–93, 162–178. <https://doi.org/10.1016/j.gloplacha.2012.05.015>
- Ikehara, K., & Itaki, T. (2007). Millennial-scale fluctuations in seasonal sea-ice and deep-water formation in the Japan Sea during the Late Quaternary. *Palaeogeography, Palaeoclimatology, Palaeoecology*, 247(1–2), 131–143. <https://doi.org/10.1016/j.palaeo.2006.11.026>
- Inoue, Y. (1989). Northwest Pacific foraminifera as paleoenvironmental indicators, science reports of the Institute of Geoscience, University of Tsukuba. *Section B, Geological Sciences*, 10, 57–162.
- Itaki, T. (2016). Transitional changes in microfossil assemblages in the Japan Sea from the late Pliocene to early Pleistocene related to global climatic and local tectonic events. *Progress in Earth and Planetary Science*, 3, 1–21.
- Itaki, T., Komatsu, N., & Motoyama, I. (2007). Orbital- and millennial-scale changes of radiolarian assemblages during the last 220 kyrs in the Japan Sea. *Palaeogeography, Palaeoclimatology, Palaeoecology*, 247(1–2), 115–130. <https://doi.org/10.1016/j.palaeo.2006.11.025>
- Jorissen, F. J. (1999). Benthic foraminiferal successions across Late Quaternary Mediterranean sapropels. *Marine Geology*, 153(1–4), 91–101. [https://doi.org/10.1016/S0025-3227\(98\)00088-7](https://doi.org/10.1016/S0025-3227(98)00088-7)
- Jorissen, F. J., de Stigter, H. C., & Widmark, J. G. V. (1995). A conceptual model explaining benthic foraminiferal microhabitats. *Marine Micropaleontology*, 26(1–4), 3–15. [https://doi.org/10.1016/0377-8398\(95\)00047-X](https://doi.org/10.1016/0377-8398(95)00047-X)
- Jorissen, F. J., Fontanier, C., & Thomas, E. (2007). Chapter seven paleoceanographical proxies based on deep-sea benthic foraminiferal assemblage characteristics. *Developments in Marine Geology*, 263–325. [https://doi.org/10.1016/S1572-5480\(07\)01012-3](https://doi.org/10.1016/S1572-5480(07)01012-3)
- Kaiho, K. (1994). Benthic foraminiferal dissolved-oxygen index and dissolved-oxygen levels in the modern ocean. *Geology*, 22(8), 719–722. [https://doi.org/10.1130/0091-7613\(1994\)022%3C0719:BFDOIA%3E2.3.CO;2](https://doi.org/10.1130/0091-7613(1994)022%3C0719:BFDOIA%3E2.3.CO;2)
- Kido, Y., Minami, I., Tada, R., Fujine, K., Irino, T., Ikehara, K., & Chun, J. H. (2007). Orbital-scale stratigraphy and high-resolution analysis of biogenic components and deep-water oxygenation conditions in the Japan Sea during the last 640 kyr. *Palaeogeography, Palaeoclimatology, Palaeoecology*, 247(1–2), 32–49. <https://doi.org/10.1016/j.palaeo.2006.11.020>
- Kitamura, A., Takano, O., Takada, H., & Omote, H. (2001). Late Pliocene–early Pleistocene paleoceanographic evolution of the Sea of Japan. *Palaeogeography, Palaeoclimatology, Palaeoecology*, 172(1–2), 81–98. [https://doi.org/10.1016/S0031-0182\(01\)00272-3](https://doi.org/10.1016/S0031-0182(01)00272-3)

- Kroon, D., Steens, T., & Troelstra, S. R. (1991). Onset of monsoonal related upwelling in the western Arabian Sea as revealed by planktonic foraminifera. In W. L. Prell, N. Niitsuma, et al. (Eds.), *Proceedings of the ocean drilling program, scientific results* (Vol. 117, pp. 257–263). College Station, TX: Ocean Drilling Program.
- Kuroyanagi, A., & Kawahata, H. (2004). Vertical distribution of living planktonic foraminifera in the seas around Japan. *Marine Micropaleontology*, 53(1–2), 173–196. <https://doi.org/10.1016/j.marmicro.2004.06.001>
- Laskar, J., Robutel, P., Joutel, F., Gastineau, M., Correia, A. C. M., & Levrard, B. (2004). A long-term numerical solution for the insolation quantities of the Earth. *Astronomy & Astrophysics*, 428(1), 261–285. <https://doi.org/10.1051/0004-6361:20041335>
- Lisiecki, L. E., & Raymo, M. E. (2005). A Pliocene-Pleistocene stack of 57 globally distributed benthic  $\delta^{18}\text{O}$  records. *Paleoceanography*, 20, PA1003. <https://doi.org/10.1029/2004PA001071>
- Matoba, Y., & Fukasawa, K. (1992). Depth distribution of recent benthic foraminifera on the continental shelf and uppermost slope off southern Akita prefecture. In *Northeast Japan (the eastern Japan Sea), centenary of Japanese micropaleontology* (pp. 207–226). Tokyo: Terra Scientific Publishing Co.
- Moriyasu, S. (1972). The Tsushima warm current. In H. Stommel & K. Yoshida (Eds.), *Kuroshio—its physical aspects* (pp. 353–369). Tokyo: Univ. of Tokyo.
- Murray, J. W. (1991). *Ecology and paleoecology of benthic foraminifera* (pp. 1–274). London: Longman Scientific and Technical.
- Murray, J. W. (2006). *Ecology and applications of benthic foraminifera* (pp. 1–426). Cambridge: Cambridge University Press. <https://doi.org/10.1017/CBO9780511535529>
- Nakagawa, T., Okuda, M., Yonenobu, H., Miyoshi, N., Fujiki, T., Gotanda, K., et al. (2008). Regulation of the monsoon climate by two different orbital rhythms and forcing mechanisms. *Geology*, 36(6), 491–494. <https://doi.org/10.1130/G24586A.1>
- Oba, T., Kato, M., Kitazato, H., Koizumi, I., Omura, A., Sakai, T., & Takayama, T. (1991). Paleoenvironmental changes in the Japan Sea during the last 85,000 years. *Paleoceanography*, 6(4), 499–518. <https://doi.org/10.1029/91PA00560>
- Ohta, A., Imai, N., Terashima, S., Tachibana, Y., Ikehara, K., & Katayama, H. (2015). Elemental distribution of surface sediments around Okai trough including adjacent terrestrial area: Strong impact of Japan Sea proper water on silty and clayey sediments. *Bulletin of the Geological Survey of Japan*, 66(3–4), 81–101. <https://doi.org/10.9795/bullgsj.66.81>
- Ortakand, M. S., Hasegawa, S., & Matsumoto, R. (2015). Biostratigraphic and palaeoecologic evaluation of the Japan Sea's Joetsu Basin based on the study of foraminifera. *Paleontological Research*, 19(2), 79–106. <https://doi.org/10.2517/2014PR031>
- Paillard, D., Labeyrie, L. D., & Yiou, P. (1996). AnalySeries 1.0: A Macintosh software for the analysis of geophysical time-series. *Eos, Transactions of the American Geophysical Union*, 77, 379.
- Peeters, F. J., Brummer, G.-J. A., & Ganssen, G. (2002). The effect of upwelling on the distribution and stable isotope composition of *Globigerina bulloides* and *Globigerinoides ruber* (planktic foraminifera) in modern surface waters of the NW Arabian Sea. *Global and Planetary Change*, 34(3–4), 269–291. [https://doi.org/10.1016/S0921-8181\(02\)00120-0](https://doi.org/10.1016/S0921-8181(02)00120-0)
- Poli, M. S., Meyers, P. A., Thunell, R. C., & Capodivacca, M. (2012). Glacial-interglacial variations in sediment organic carbon accumulation and benthic foraminiferal assemblages on the Bermuda Rise (ODP site 1063) during MIS 13 to 10. *Paleoceanography*, 27, PA3216. <https://doi.org/10.1029/2012PA002314>
- Qiu, B. (2001). Kuroshio and Oyashio currents. In J. H. Steele, S. A. Thorpe, & K. K. Turekian (Eds.), *Encyclopedia of ocean sciences* (pp. 1413–1425). London: Academic Press. <https://doi.org/10.1006/rwos.2001.0350>
- Railsback, L. B., Gibbard, P. L., Head, M. J., Voarintsoa, N. R. G., & Toucanne, S. (2015). An optimized scheme of lettered marine isotope substages for the last 1.0 million years, and the climatostratigraphic nature of isotope stages and substages. *Quaternary Science Reviews*, 111, 94–106. <https://doi.org/10.1016/j.quascirev.2015.01.012>
- Sagawa, T., Nagahashi, Y., Satoguchi, Y., Holbourn, A., Itaki, T., Gallagher, S. J., et al. (2018). Integrated tephrostratigraphy and isotope stratigraphy in the Japan Sea and East China Sea using IODP sites U1427, U1426 and U1429, Expedition 346 Asian monsoon. *Progress in Earth and Planetary Science*, 5, 18. <https://doi.org/10.1186/s40645-018-0168-7>
- Shannon, C. E., & Weaver, W. (1949). *The mathematical theory of communication* (p. 125). Illinois: University of Illinois Press.
- Smith, V. C., Staff, R. A., Blockley, S. P. E., Bronk Ramsey, C., Nakagawa, T., Mark, D. F., et al. (2013). Identification and correlation of visible tephra in the Lake Suigetsu SG06 sedimentary archive, Japan: Chronostratigraphic markers for synchronising of East Asian/West Pacific palaeoclimatic records across the last 150 ka. *Quaternary Science Reviews*, 67, 121–137. <https://doi.org/10.1016/j.quascirev.2013.01.026>
- Spratt, R. M., & Lisiecki, L. E. (2016). A late Pleistocene sea level stack. *Climate of the Past*, 12(4), 1079–1092. <https://doi.org/10.5194/cp-12-1079-2016>
- Suda, K. (1932). On the bottom water in the Japan Sea (preliminary report) [in Japanese]. *Journal of the Oceanographical Society of Japan*, 4, 221–241.
- Sun, Y., Kutzbach, J., An, Z., Clemens, S., Liu, Z., Liu, W., et al. (2015). Astronomical and glacial forcing of East Asian summer monsoon variability. *Quaternary Science Reviews*, 115, 132–142. <https://doi.org/10.1016/j.quascirev.2015.03.009>
- Tada, R. (1994). Paleoceanographic evolution of the Japan Sea. *Palaeogeography, Palaeoclimatology, Palaeoecology*, 108(3–4), 487–508. [https://doi.org/10.1016/0031-0182\(94\)90248-8](https://doi.org/10.1016/0031-0182(94)90248-8)
- Tada, R. (2004). Onset and evolution of millennial-scale variability in the Asian monsoon and its impact on paleoceanography of the Japan Sea. In *Continent-ocean interactions within East Asian marginal seas* (pp. 283–298). Washington, DC: American Geophysical Union. <https://doi.org/10.1029/149GM15>
- Tada, R., Irino, T., Ikehara, K., Sugisaki, A., Sagawa, C. X. T., Itaki, T., et al. (2018). High-resolution and -precision correlation of dark and light layers in the Quaternary hemipelagic sediments of the Japan Sea recovered during IODP Expedition 346. *Progress in Earth and Planetary Science*, 5, 19. <https://doi.org/10.1186/s40645-018-0167-8>
- Tada, R., Irino, T., & Koizumi, I. (1999). Land-ocean linkages over orbital and millennial timescales recorded in Late Quaternary sediments of the Japan Sea. *Paleoceanography*, 14(2), 236–247. <https://doi.org/10.1029/1998PA000016>
- Tada, R., Murray, R., Zarkian, C. A., & Exp. 346 Scientists (2015a). *Expedition 346 summary, proc. IODP, 346*. College Station, TX: Integrated Ocean Drilling Program.
- Tada, R., Murray, R., Zarkian, C. A., & Exp. 346 Scientists (2015b). *Site U1427, proc. IODP, 346*. College Station, TX: Integrated Ocean Drilling Program.
- Tada, R., Oba, T., & Jordan, R. W. (2007). Preface for special volume: "Quaternary paleoceanography of the Japan Sea and its linkage with Asian monsoon". *Palaeogeography, Palaeoclimatology, Palaeoecology*, 247(1–2), 1–4. <https://doi.org/10.1016/j.palaeo.2006.11.017>
- Takikawa, T., & Yoon, J.-H. (2005). Volume transport through the Tsushima Straits estimated from sea level difference. *Journal of Oceanography*, 61(4), 699–708. <https://doi.org/10.1007/s10872-005-0077-4>
- Ujiié, H., Ichikura, M., & Kurihara, K. (1983). Upward decrease of organic C/N ratios in the Okinawa trough cores: Proxy for tracing the post-glacial retreat of the continental shore line. *Bulletin National Science Museum, Tokyo, Series C*, 9, 41–80.

- Usami, K., Ohi, T., Hasegawa, S., & Ikehara, K. (2013). Foraminiferal records of bottom-water oxygenation and surface-water productivity in the southern Japan Sea during 160-15ka: Associations with insolation changes. *Marine Micropaleontology*, 10110–10127.
- van Hinsbergen, D., Kouwenhoven, T., & Van der Zwaan, G. (2005). Paleobathymetry in the backstripping procedure: Correction for oxygenation effects on depth estimates. *Palaeogeography, Palaeoclimatology, Palaeoecology*, 221(3-4), 245–265. <https://doi.org/10.1016/j.palaeo.2005.02.013>
- Wallace, M. W., Holdgate, G. R., Daniels, J., Gallagher, S. J., & Smith, A. (2002). Sonic velocity, submarine canyons, and burial diagenesis in Oligocene-Holocene cool-water carbonates, Gippsland Basin, Southeast Australia. *AAPG Bulletin*, 86, 1593–1607.
- Watanabe, S., Tada, R., Ikehara, K., Fujine, K., & Kido, Y. (2007). Sediment fabrics, oxygenation history, and circulation modes of Japan Sea during the Late Quaternary. *Palaeogeography, Palaeoclimatology, Palaeoecology*, 247(1-2), 50–64. <https://doi.org/10.1016/j.palaeo.2006.11.021>
- Zheng, W., De Vleeschouwer, D., Shen, J., Zhang, Z., & Zeng, L. (2018). Orbital time scale records of Asian eolian dust from the Sea of Japan since the early Pliocene. *Quaternary Science Reviews*, 187, 157–167. <https://doi.org/10.1016/j.quascirev.2018.03.004>